Cacnb4 directly couples electrical activity to gene expression, a process defective in juvenile epilepsy.

Abir Tadmouri, Shigeki Kiyonaka, Maud Barbado, Matthieu Rousset, Katell Fablet, Seishiro Sawamura, Eloi Bahembera, Karin Pernet-Gallay, Christophe Arnoult, Takafumi Miki, et al.

Cacnb4 directly couples electrical activity to gene expression, a process defective in juvenile epilepsy

Running title: *Cacnb4, an adaptor protein for gene regulation*

Abir Tadmouri[1*], Shigeki Kiyonaka[2*], Maud Barbado[1,3*], Matthieu Rousset[4,5*], Katell Fablet[1*], Seishiro Sawamura[2], Eloi Bahembera[1,3], Karin Pernet-Gallay[1], Christophe Arnoult[1], Takafumi Miki[2], Karin Sadoul[6], Sylvie Gory-Faure[1], Caroline Lambrecht[7], Florian Lesage[3,8], Satoshi Akiyama[2], Saadi Khochbin[6], Sylvain Baulande[9], Veerle Janssens[7], Annie Andrieux[1], Ricardo Dolmetsch[4], Michel Ronjat[1,3⊕], Yasuo Mori[2] and Michel De Waard[1,3,⊕]

[1]Unité Inserm U836, Grenoble Institute of Neuroscience, Université Joseph Fourier, Site Santé, 38700 La Tronche, France.

[2]Laboratory of Molecular Biology, Department of Synthetic Chemistry and Biological Chemistry, Graduate School of Engineering, Kyoto University, Kyoto 615-8510, Japan.

[3]LabEx ICST 'Ion Channel Science and Therapeutics'.

[4]Department of Neurobiology, Stanford University School of Medicine, 299 Campus Drive, Stanford, CA 94305, USA.

[5]CRBM, CNRS UMR5237, 34293 Montpellier, France.

[6]Inserm U823, Institut Albert Bonniot, Grenoble, France.

[7]Laboratory of protein phosphorylation and proteomics, University of Leuven, PO-box 901, B-3000, Leuven, Belgium.

[8]Institut de Pharmacologie Moléculaire et Cellulaire, Sophia Antipolis, F-06560 Valbonne, France.

[9]PartnerChip, Bat. G2, 2, rue Gaston Crémieux, 91000 Evry, France.

[*]These authors contributed equally to this work.

[⊕] Contacts: Dr. Michel De Waard - Tel.: (33) 4 56 52 05 63 – Fax: (33) 4 56 52 05 72 – E-mail: michel.dewaard@ujf-grenoble.fr & Dr. Michel Ronjat – Tel. : (33) 4 56 52 05 64 – E-mail : michel.ronjat@ujf-grenoble.fr

Calcium current through voltage-gated calcium channels (VGCC) controls gene expression. Here, we describe a novel signaling pathway in which the VGCC Cacnb4 subunit directly couples neuronal excitability to transcription. Electrical activity induces Cacnb4 association to Ppp2r5d, a regulatory subunit of PP2A phosphatase, followed by i) nuclear translocation of Cacnb4/Ppp2r5d/PP2A, ii) association with the tyrosine hydroxylase (TH) gene promoter through the nuclear transcription factor thyroid hormone receptor alpha (TRα), and iii) histone binding through association of Cacnb4 with HP1γ concomitantly with Ser^{10} histone H3 dephosphorylation by PP2A. This signaling cascade leads to TH gene repression by Cacnb4 and is controlled by the state of interaction between the SH3 and guanylate kinase (GK) modules of Cacnb4. The human R482X CACNB4 mutation, responsible for a form of juvenile myoclonic epilepsy, prevents association with Ppp2r5 and nuclear targeting of the complex by altering Cacnb4 conformation. These findings demonstrate that an intact VGCC subunit acts as a repressor recruiting platform to control neuronal gene expression.

Keywords: β4 subunit / Gene regulation / thyroid receptor alpha / phosphatase 2A / HP1γ

Introduction

Voltage-gated calcium channels (VGCC) are heteromultimeric complexes that translate electric signals into calcium influx (Catterall et al, 2005), thereby controlling synaptic vesicle exocytosis, neuronal excitability and gene expression (Deisseroth et al, 2003; Flavell & Greenberg, 2008; Greer & Greenberg, 2008). In VGCC, the pore-forming subunit is associated to auxiliary subunits, among which the cytoplasmic Cacnb4

(β_4) plays an essential function in channel expression level at the plasma membrane and biophysical properties (Arikkath & Campbell, 2003). Mutations in the genes encoding VGCC induce diverse neuronal pathologies, such as epilepsy, ataxia, autism, and migraine (Bidaud et al, 2006). In humans, a mutation of *CACNB4*, leading to a 38 amino acid truncation of β_4 C-terminus, has been associated to juvenile myoclonic epilepsy (Escayg et al, 2000). In mice, a four-nucleotide insertion into a splice donor site of *Cacnb4* results in a truncation of 60% of the protein sequence and a *lethargic* (*lh*) phenotype (Burgess et al, 1997). How these mutations may affect VGCC-mediated function still remains an open question. Calcium entering through VGCC has been implicated in gene regulation by activating calcium-binding proteins that propagate the signal to the nucleus (Dolmetsch et al, 2001; Graef et al, 1999; Oliveria et al, 2007; Rosen et al, 1994) or by diffusing to the nucleus with or without signal amplification by intracellular stores (Carrion et al, 1999; Hardingham et al, 2001; Hardingham et al, 1997). Evidences for alternative pathways have been reported. First, an atypical short β_4 splice variant, β_{4c}, was shown to interact with heterochromatin protein 1 gamma (HP1γ), a nuclear protein involved in gene silencing and transcription regulation (Hibino et al, 2003; Xu et al, 2011). However, β_{4c} lacks the domain required for association with the pore subunit (Chen et al, 2004) and therefore cannot couple neuronal activity to gene regulation. A second pathway implicates CCAT, a C-terminal fragment of Cacna1c VGCC, as a calcium-regulated transcription factor (Gomez-Ospina et al, 2006). In this case, calcium influx triggers CCAT nuclear export providing a calcium-dependent link between neuronal activity and transcription. The origin of this fragment (channel proteolysis or alternative splicing) remains unknown.

Here, we show that β_4 directly couples neuronal excitability to gene expression along a signaling pathway that is disrupted by the human R482X mutation. We found that electrical activity promotes the formation of a new nuclear complex in which β_4 plays the role of an organizing platform that brings together a transcription factor for DNA binding, a phosphatase for histone dephosphorylation and HP1γ for nucleosome association. Formation of this complex controls gene activity as witnessed by the case of tyrosine hydroxylase (TH) gene.

Results

β_4 nuclear localization

β_4 is highly expressed in the hippocampal dentate gyrus of adult wild-type (wt) C57Bl/6 mice brain but not in *lh* mice brain (Figure 1a). β_4 labeling is strongest in soma and coincides with NeuN nuclear labeling, suggesting that a fraction of β_4 protein may be localized in cell nuclei, in agreement with previous observations (Subramanyam et al, 2009). Western blot analyses of wt brain lysates show a unique 58 kDa band, corresponding to β_4, absent in *lh* (Figure 1b). Western blot analyses of cytoplasmic *versus* nuclear fractions of wt brain lysates show the presence of β_4 in the nucleus (Figure 1c). Electron microscopy (EM) demonstrates the presence of β_4 in the nucleus of CA1 hippocampal neurons (Figure 1d & Supplementary Figure 1). In primary cultures of hippocampal neurons, β_4 is predominantly expressed within the cytoplasm/plasma membrane at 5 DIV (Figure 1e, left panels). In contrast, the protein is densely located in the nucleus at 18 DIV (Figure 1e, right panels). The nuclear to cytoplasmic density ratios (NCR values) of β_4 increases as a function of time from 0.07 (3 DIV) to 3.81 (18 DIV) on

average indicating the differentiation-dependent progressive targeting of β_4 to neuronal nuclei (Figure 1f). NCR value increase is accompanied by a histogram broadening witnessing higher β_4 subcellular distribution variability among neurons. β_4 nuclear appearance coincides with that of VGCC currents and electrical activity at 5 DIV (unpublished observation). EM analysis of hippocampal neurons at 5 and 18 DIV also illustrate the increase of β_4 nuclear density at 18 DIV (Figure 1g). Synchronized neuronal differentiation of NG108-15 cells, induced by serum deprivation and 1 mM cAMP, is accompanied by VGCC expression (Chemin et al, 2002). In undifferentiated NG108.15 cells, β_4 is exclusively cytoplasmic, while present in nuclei after 13 days of differentiation (Figure 1h). Mean NCR values illustrate that nuclear β_4 expression is triggered by neuronal differentiation (Figure 1i).

β_4 epilepsy mutation alters nuclear targeting

To search for a β_4 nuclear targeting domain, truncated β_4-EGFP constructs were expressed in CHO cells (Figure 2a). In CHO and HEK293 cells, β_4-EGFP spontaneously locates in the nucleus (NCR = 10.1 ± 3.3 for CHO cells). In contrast, truncated constructs are deficient in nuclear targeting suggesting that β_4 has no nuclear localization sequence (NLS) or that the NLS sequence depends on β_4 structure integrity (Figure 2b,c). Indeed, five constructs display a distribution similar to EGFP alone (NCR ~1). Two constructs, that contain β_4 guanylate kinase (GK) domain, show preferential cytoplasm distribution (NCR = 0.27 ± 0.2 and 0.26 ± 0.2 for $\beta_{216\text{-}402}$-EGFP and $\beta_{216\text{-}519}$-EGFP, respectively). β_4-EGFP truncation therefore results in 10 to 40-fold decrease of nuclear targeting efficiency. These data were confirmed for two truncated β_4 constructs by Western blot

analyses of nuclear and cytoplasmic fractions of transfected HEK293 cells (Supplementary Figure 2a). An earlier report mentioned the importance of a restricted N-terminal domain for β_4 nuclear accumulation (Subramanyam et al, 2009). As observed in this study, mutation of this domain significantly reduced nuclear accumulation albeit by a limited extent (by 1.41-fold, from a mean NCR value of 11.4 ± 0.7 to 8.1 ± 0.7). However, $\beta_{R28A\text{-}R29A\text{-}S30A}$-EGFP still significantly accumulates into the nucleus in contrast to the constructs presented in this manuscript.

We engineered a $\beta_{1\text{-}481}$-EGFP mutant (Figure 2a) corresponding to the human juvenile myoclonic epilepsy mutation (Escayg et al, 2000) and assessed its cellular distribution in CHO cells (Figure 2b,c). Nuclear accumulation of $\beta_{1\text{-}481}$-EGFP mutant is strongly reduced (NCR = 0.98 ± 0.62; 10.3-fold lower than β_4-EGFP NCR). This mutation induces a loss in nuclear targeting as shown by Western blot analyses of nuclear and cytoplasmic fractions of CHO cells (Figure 2d). Finally, $\beta_{1\text{-}481}$-EGFP mutant is completely excluded from hippocampal neuron nuclei at 7 DIV (NCR = 0.32 ± 0.18; Figure 2e,f). This corresponds to a 9.5-fold decrease in NCR value compared to β_4-EGFP (3.15 ± 1.76), a reduction similar to that measured in CHO cells. Double imaging of immunolabeled endogenous β_4 and $\beta_{1\text{-}481}$-EGFP indicates the extent of nuclear exclusion of the mutant (Figure 2g). In conclusion, the nuclear targeting of β_4 requires the preservation of its structural integrity. The human epilepsy mutation alters this structural integrity and hinders nuclear targeting.

The SH3/GK interaction controls β_4 nuclear targeting

Interaction between β SH3 and GK domains regulates channel activity (McGee et al, 2004; Takahashi et al, 2005). Its role was therefore investigated on β_4 nuclear targeting. Three constructs were designed: $\beta_{1\text{-}166}$-EGFP, $\beta_{200\text{-}519}$-myc, and $\beta_{200\text{-}481}$-myc (corresponding to the juvenile epilepsy deletion) (Figure 3a). In agreement with Figure 2c, none of these constructs show a specific nuclear targeting in CHO cells (Figure 3b). Expressed together, $\beta_{1\text{-}166}$-EGFP and $\beta_{200\text{-}519}$-myc reconstitute a nuclear-targeting-competent complex (Figure 3c; NCR = 6.9 ± 1.6 for $\beta_{1\text{-}166}$-EGFP, and 7.1 ± 1.1 for $\beta_{200\text{-}519}$-myc). In contrast, expression of $\beta_{1\text{-}166}$-EGFP with $\beta_{200\text{-}481}$-myc fails to form a nuclear complex (Figure 3c, right panels). Co-immunoprecipitation experiments show that $\beta_{200\text{-}481}$-myc no longer interacts with $\beta_{1\text{-}166}$-EGFP contrary to $\beta_{200\text{-}519}$-myc (Figure 3d). These data suggest that the human mutation prevents β_4 nuclear targeting by modulating the SH3/GK interaction. This issue was further addressed by investigating the effect of two mutations (SH3 L125P or GK P225R) known to disrupt the SH3/GK interaction (McGee et al, 2004; Takahashi et al, 2004) (Figure 3e). As shown, $\beta_{1\text{-}166\text{-}L125P}$-EGFP no longer interacts with $\beta_{200\text{-}519}$-myc (Figure 3f). Also, both β_{L125P}-EGFP and β_{P225R}-EGFP are completely excluded from hippocampal neuron nuclei (Figure 3g). NCR values, 0.43 ± 0.15 (L125P) and 0.43 ± 0.11 (P225R), correspond to a 7.3-fold decrease in mutant β_4 nuclear localization (Figure 3h). These results demonstrate that β_4 nuclear targeting requires the internal SH3/GK and reveal a previously unrecognized structural role of the last C-terminal 38 amino acid sequence in modulating the interaction between the C-terminal containing hemi-β_4 subunit and the SH3-containing β_4 fragment.

The phosphatase 2A Ppp2r5d (B56δ) subunit contributes to β_4 nuclear localization

Absence of a clear molecular determinant for β_4 nuclear targeting, suggests that this process requires at least one protein partner, whereas defective $\beta_{1\text{-}481}$, β_{L125P} and β_{P225R} nuclear localization indicates that interaction with this (these) partners depends on SH3/GK interaction state. Yeast two-hybrid screenings were performed with a mouse brain complementary DNA library using β_4 as bait. The 62 positive clones were subjected to two-hybrid β-galactosidase assays using β_4 and $\beta_{1\text{-}481}$ as baits. B56δ, a 594 amino acid protein containing a poorly-defined NLS at its C-terminus, was revealed to interact with β_4 but not with $\beta_{1\text{-}481}$ (Figure 4a). B56δ is one of the two regulatory subunits of phosphatase 2A (PP2A), along with B56γ, known to target PP2A to the nucleus (McCright et al, 1996). Co-immunoprecipitation confirms that β_4-EGFP, but not $\beta_{1\text{-}481}$-EGFP, interacts with B56δ-myc expressed in HEK293 cells (Figure 4b). As expected, Cacna1e and RIM1 were also identified as β_4 partners (Kiyonaka et al, 2007). In contrast to B56δ, both proteins interact equally well with β_4 and $\beta_{1\text{-}481}$. These yeast two-hybrid assays also reveal that Cacnb3 (β_3), another β isoform, also interacts with B56δ suggesting the existence of redundant signaling pathways (Figure 4c). β_{4c}, a short β_4 splice variant, known to interact with the HP1γ chromo shadow domain (Hibino et al, 2003), does not interact with B56δ. Conversely, β_4 does not interact with HP1γ in these conditions (Figure 4c). Truncated β_4 constructs were analyzed for B56δ interaction by yeast two-hybrid assays (Figure 4d). $\beta_{49\text{-}519}$ is the only truncated construct interacting with B56δ indicating that the N-terminus is not essential for this interaction. B56δ does not interact with β_{L125P} confirming that binding to β_4 requires an intact SH3/GK interaction (Figure 4d). Endogenous B56δ is expressed in both HEK293 and CHO cells

in agreement with spontaneous nuclear targeting of β_4 (Supplementary Figure 3a,b). Exogenous B56δ-myc co-localizes with nuclear β_4-EGFP and further increases β_4-EGFP nuclear targeting in CHO cells (Supplementary Figure 3c). Conversely, expression of a B56δ shRNA, reducing the level of endogenous B56δ in CHO cells (Supplementary Figure 3b), leads to a reduction of β_4-EGFP nuclear targeting (NCR value dropping from 11.5 ± 0.7 to 7.3 ± 0.5 or average 4.3-fold redistribution between nuclear and cytoplasmic pools by WB) (Figure 4e,f). In agreement with binding data, B56δ-myc expression has no effect on $\beta_{1\text{-}481}$-EGFP distribution in CHO cells (Supplementary Figure 3d). Expression of B56δ-myc in non-differentiated NG108-15 cells produces a marked nuclear re-localization of endogenous β_4 (Figure 4g; 11.8-fold increase in NCR). The influence of B56δ on endogenous β_4 nuclear localization was further investigated using B56δ$^{-/-}$ mice (Louis et al, 2011). Hippocampal neurons from B56δ$^{-/-}$ mice show a significant 1.65-fold decrease in NCR value at 11 DIV (Figure 4h). Similarly, the density of immunogold-labeled endogenous β_4 is significantly decreased by 1.61-fold in B56δ$^{-/-}$ adult hippocampal neurons compared to wt hippocampal neurons (Figure 4i). In conclusion, B56δ is a SH3/GK conformation-sensitive β_4 partner that contributes to nuclear distribution of β_4. Since a fraction of β_4 is still nuclear in the absence B56δ, we conclude that other B56 isoforms and/or nuclear partners also help β_4 accumulation in neuronal nuclei. $\beta_{1\text{-}481}$ deficient nuclear targeting originates from its inability to interact with B56δ.

β_4 forms a complex with B56δ and active PP2A

Immunoprecipitation of endogenous β_4 from wt mice brain results in coprecipitation of B56δ and PP2A (Figure 5a). As expected, neither B56δ nor PP2A are immunoprecipitated from *lh* mice brain by β_4 antibodies. Similarly, PP2A is not precipitated by β_4 antibodies using B56$\delta^{-/-}$ mice brain indicating that PP2A/β_4 association requires B56δ. In HEK293 cells, over-expression of B56δ-EGFP with β_4-myc strongly enhances endogenous PP2A immunoprecipitation through β_4-myc (Figure 5b). Restricted immunoprecipitation of endogenous PP2A by antibodies against β_4-myc suggests that not all endogenous B56δ (Supplementary Figure 3a) is associated to PP2A in these cells, possibly due to a competition with other B regulatory isoforms unable to associate to β_4-myc. As expected, $\beta_{1\text{-}481}$-myc mutant does not precipitate endogenous PP2A in the presence of B56δ-EGFP (Figure 5b). β_4-myc/B56δ-EGFP complex immunoprecipitated from HEK293 cells shows PP2A phosphatase activity (Figure 5c).

Membrane depolarization triggers β_4 association to B56δ

β_4-EGFP, expressed together with Cacna1a and Cacna2d2, pore-forming and auxiliary subunits of VGCC, loses its nuclear distribution in HEK293 cells (Figure 5d, NCR = 0.25 ± 0.1, i.e. 40-fold reduction). Part of β_4-EGFP staining is cytoplasmic instead of at the plasma membrane, possibly by interaction with Cacna1a stuck in the endoplasmic reticulum. As expected, $\beta_{1\text{-}481}$-EGFP mutant distribution remains cytoplasmic in the presence of VGCC (Figure 5d, right panel). In the presence of Cacna1a and Cacna2d2, B56δ-myc no longer interacts with β_4-EGFP (Figure 5e). These data indicate that (i) B56δ does not form a higher order molecular complex with the channel and (ii) β_4

association to Cacna1a overrides its interaction with B56δ. In addition, B56δ-EGFP does not affect VGCC kinetics and current densities in HEK293 cells (Supplementary Figure 4a,b). Also, Ca^{2+} currents were not modified in hippocampal neurons from B56δ$^{-/-}$ mice (Supplementary Figure 4c,d), confirming that B56δ does not associate to the channel complex. Previous reports evidenced that β/channel interaction is reversible (Restituito et al, 2001; Sandoz et al, 2004; Spafford et al, 2004), but the impact of membrane depolarization on this interaction has not been studied. Membrane depolarization of HEK293 cells enhances β_4-myc interaction with B56δ-EGFP, while it does not promote any interaction between $\beta_{1\text{-}481}$-myc and B56δ-EGFP (Figure 5f). In the presence of VGCC, the depolarization-induced B56δ-myc/β_4-EGFP interaction requires external Ca^{2+} (Supplementary Figure 5). In these conditions, β_4-myc precipitates endogenous PP2A only upon membrane depolarization (Figure 5g). In contrast, $\beta_{1\text{-}481}$-myc does not precipitate PP2A upon depolarization. Finally, blocking electrical activity of 11 DIV hippocampal neurons by 1 μM tetrodotoxin (TTX) produces a significant 2.1-fold reduction of β_4 NCR value measured at 18 DIV (Figure 5h). This TTX effect is not observed in B56δ$^{-/-}$ hippocampal neurons, demonstrating that β_4 nuclear accumulation induced by electrical activity relies on B56δ. Note the 2.45-fold reduction in NCR value between wt and B56δ$^{-/-}$ control neurons at 18 DIV in agreement with B56δ role in β_4 nuclear accumulation. Conversely, a 1 hr stimulation of neuronal electric activity by a biccuculine/4-AP cocktail produces a significant 23.5 ± 1.9% increase in NCR value that is not observed in B56δ$^{-/-}$ hippocampal neurons (Figure 5i). Depolarization of the plasma

membrane therefore represents an important signaling event that allows β_4/B56δ interaction and favors β_4 nuclear accumulation.

β_4 represses TH gene expression by interacting with the thyroid hormone receptor alpha

To determine whether β_4 regulates transcription of endogenous genes, we analyzed a publicly available microarray data set comparing gene expression in wt and *lh* mice cerebellum (data set GSE6275 from Gene Expression Omnibus, http://www.ncbi.nlm.nih.gov/geo). A volcano plot representation of our statistical analysis identifies 56 up-regulated and 38 down-regulated genes (over twofold expression change, $p<0.05$) in *lh* mice cerebellum (Supplementary Figure 6). Based on gene ontology annotations, clustering of regulated transcripts in functional groups illustrate that many encode proteins with functions related to signaling and ion transport (Supplementary Figure 6). Among these genes, those coding for TH and for BC031748 cDNA sequence are the most up- and down-regulated, respectively (Figure 6a). The effect of β_4 on gene expression was confirmed on a set of genes by qRT-PCR experiments using purified mRNA from wt and *lh* mice cerebellum (Figure 6b). From both approaches, TH gene shows the greatest variation in expression level; an interesting observation considering its relevance in epilepsy (Bengzon et al, 1999; Donato et al, 2006; Hess & Wilson, 1991). The up-regulation of TH expression in *lh* mice cerebellum indicates that β_4 acts as a repressor on this gene. Transcripts up- or down-regulation is lost in the hippocampus and in the cortex indicating the existence of compensatory mechanisms to the lack of β_4. Interaction of β_4 with the promoter region of TH gene was

investigated by chromatin immunoprecipitation (ChIP) experiments. ChIP of the TH gene promoter from hippocampal neurons in culture, using antibodies against β_4, shows specific precipitation at 18 DIV but not 1 DIV (Figure 6c). As a control, ChIP of the 3'-UTR region of TH gene were negative at 18 DIV. Similar results were obtained for ChIP experiments of the transmembrane protein 100 gene promoter (Supplementary Figure 7), suggesting that the TH promoter is not an isolated case. In wt mice brain, β_4 antibodies immunoprecipitate 1.89 ± 0.42% of TH promoter input, corresponding to a 6.3-fold enrichment over control (Figure 6d). In contrast, no specific TH promoter immunoprecipitation is observed using *lh* mice brain (Figure 6d). β_4 antibodies also immunoprecipitate 1.37 ± 0.06% of TH promoter from B56$\delta^{-/-}$ mice, indicating that β_4 association with the promoter does not necessarily require the B56δ partner (3.3-fold enrichment; Supplementary Figure 8a). Yeast two hybrid screening, using β_4 as bait, was used to identify a transcription factor that targets β_4 to the TH gene. The thyroid hormone receptor alpha (TRα) came out as a positive candidate (Figure 6e). TRα is a nuclear receptor that contains a T3 hormone binding domain and a DNA binding domain interacting with Thyroid Receptor Elements (TRE). Interaction of TRα with β_4 was confirmed by coimmunoprecipitation experiments in HEK293 cells (Figure 6f). However, this interaction is barely detectable in wt brain lysates probably because it constitutes a minor interacting fraction of total brain β_4 (not shown). ChIP using TRα antibodies show that TRα can interact with the TH gene promoter regardless of the presence of β_4 or B56δ (Figure 6g). Enrichments of the TH gene promoter were 4.92-, 4.77- and 4.27-fold for wt, *lh* and B56δ KO brains, respectively. This result is in agreement with the presence of putative TRE in the promoter region and in the coding

sequence of the TH gene. The effect of TRα on TH gene promoter was tested using a luciferase reporter (Figure 6h). TRα has little effect on its own on the expression of luciferase, while its activation by the T3 hormone leads to a 4.4-fold repression of luciferase expression (Figure 6h). Interestingly, β_4, like T3, activates the repressing function of TRα (4.8-fold repression). The effect of β_4 on TRα activity may therefore constitute a first step of TH gene repression in agreement with the up-regulation of this gene in the cerebellum in the absence of β_4.

B56δ induces the recruitment of HP1γ by β4 and contributes to association of the signaling complex with histones

ChIP experiments using B56δ antibodies reveal the presence of B56δ within the β_4 complex associated to the promoter of the TH gene (Figure 7a). Control experiments using B56δ KO mice brain demonstrate the specificity of the signal, while the absence of TH precipitation in *lh* brain denotes a key role of β_4 in targeting B56δ to the TH promoter. The presence of PP2A in the complex associated to the TH promoter was also confirmed by using PP2A antibodies (Figure 7b). TH promoter precipitation by PP2A antibodies was diminished in *lh* brain indicating the importance of β_4 in recruiting PP2A to the TH gene (Supplementary Figure 8b). Next, we questioned the role of B56δ and PP2A in TH gene regulation. Phosphorylation of histones regulates chromatin state and gene transcription (Jenuwein & Allis, 2001). Within the nucleus of wt CA1 hippocampal neurons, 45% of β_4 gold-labeled is associated to heterochromatin (black arrows; n=195/440, Figure 1d), whereas the remaining fraction is associated to euchromatin. Expression of B56δ-EGFP together with β_4-myc in HEK293 cells leads to a genome-

wide dephosphorylation of Ser^{10} of histone H3 (Figure 7c), in agreement with earlier findings that PP2A dephosphorylates histone H3 (Nowak et al, 2003). This effect cannot be attributed to an increased population of transfected cells in G2/M phases of the cell cycle (Supplementary Figure 8c). In addition, immunoprecipitated β_4-myc/B56δ-EGFP/PP2A-HA complex allows dephosphorylation of a Ser^{10} phosphorylated histone H3 N-terminal peptide (Figure 7d). Finally, ChIP experiments using anti-histone H3 and anti-phosphorylated H3 Ser^{10} antibodies shows that the absence of β_4 in *lh* brain is accompanied by an increase of histone H3 Ser^{10} phosphorylation at the TH promoter (Figure 7e). Ser^{10} dephosphorylation of histone H3 has been associated to recruitment of HP1γ (Fischle et al, 2005). Interestingly, HP1γ has been shown to interact with a PXVXV motif on β_{4c} (Xu et al, 2011), a short splice variant of β_4. Although this motif is also found in full length β_4 (Figure 7f), no interaction with HP1γ has been detected by yeast two hybrid (Figure 4c and ref. (Hibino et al, 2003)). Nevertheless, we questioned whether the interaction of β_4 with B56δ could control its interaction with HP1γ. Indeed, expression of B56δ-EGFP strongly enhances immunoprecipitation of HP1γ-EGFP by β_4-myc (Figure 7g). The basal level of precipitation of HP1γ-EGFP by β_4-myc is due to the presence of endogenous B56δ in HEK293 cells (Supplementary Figure 3a). The B56δ-dependence of HP1γ/β_4 interaction, together with the PP2A-induced dephosphorylation of histone H3 Ser^{10}, prompted us to investigate the interaction of this complex with histones. Immunoprecipitation of mice brain β_4 leads to the precipitation of histone H3 (Figure 7h). The specificity of this association is witnessed by the lack of histone H3 precipitation from *lh* brain. Importantly, β_4 association with histone H3 is lost in $B56\delta^{-/-}$ mice brain, in agreement with the specific role of B56δ in β_4/HP1γ interaction. In

HEK293 cells, immunoprecipitation of β_4-myc leads to the co-precipitation of all histones (H2B, H3 and H4) (Figure 7i), constitutive of nucleosomes. This is in agreement with the endogenous expression of B56δ (Supplementary Figure 3a) and HP1γ (Supplementary Figure 3d) in these cells. Expression of B56δ further enhances β_4-myc/histone interaction (Figure 7i). Similarly, B56δ-myc requires the expression of β_4-EGFP to precipitate histone H3, in agreement with the fact that HP1γ binds β_4 and not B56δ (Figure 7j). B56δ-myc expressed together with β_{L125P}-EGFP or $\beta_{1\text{-}481}$-EGFP mutants, deficient for B56δ association, no longer precipitate histone H4 further supporting the B56δ-dependence of β_4/HP1γ interaction (Figure 7k). Neuronal differentiation strongly increases the association of endogenous β_4 with histone H3 in NG108-15 (Supplementary Figure 9a), which correlates with the differentiation-dependent β_4 nuclear targeting (Figure 1h,i). In the presence of B56δ-EGFP and channel subunits, membrane depolarization increases β_4-myc, but not $\beta_{1\text{-}481}$-myc, association to histone H3 (Supplementary Figure 9b). Coherent with its role as PP2A regulatory subunit and its genome-wide effect observed in Figure 7c, B56δ-EGFP expression in HEK293 cells results also in dephosphorylation of Ser^{10} of β_4-myc-associated histone H3 (Supplementary Figure 9c). ChIPs experiments using anti-HP1γ antibodies demonstrate the association of HP1γ to the TH promoter (Figure 7l). The strong decrease of this association in *lh* brain illustrates the role of β_4 in recruiting HP1γ to the TH gene. Finally, double mutation of the HP1γ binding motif of β_4 precludes the B56δ-dependent interaction of β_4 with histone H3 demonstrating that HP1γ or HP1γ-like proteins are required for β_4 association to histones (Figure 7m).

β4-dependent TH gene repression is mediated by electrical activity

Our results indicate that in neurons there should be a β_4-dependent coupling between electrical activity and TH gene repression. To validate this conclusion, the electrical activity-dependence of TH mRNA levels was investigated using cerebellar granule neurons from wt and *lh* mice. Because these cells required depolarizing conditions to survive (25 mM KCl), which promotes basal level electrical activity, our control condition was defined as TH mRNA level after 2 days of TTX treatment (from 8 DIV to 10 DIV). Promoting electrical activity for one day, by removing TTX from 9 DIV to 10 DIV, induces strong TH mRNA level repression in wt (50%) but not in *lh* neurons (Figure 8a).

Discussion

Here, we characterized a novel signaling pathway in which, under membrane depolarization, the VGCC β_4 subunit accumulates in the nucleus and acquires a gene regulatory function by successively recruiting the B56δ/PP2A complex, a transcription factor and the heterochromatin protein HP1γ. Nuclear localization of β_4 was previously shown in mice brain by Subramanyam and coll. (Subramanyam et al, 2009). In contrast to what we observe with endogenous β_4, these authors show that depolarization of cultured neurons expressing V5-tagged β_4 promotes nuclear export of the tagged protein. Besides the possibility that the V5 tag may interfere with the β_4 / B56δ interaction we describe and thus modify β_4 nuclear targeting pathways, these results may highlight an active equilibrium between different pathways of β_4 nuclear import and export. This

group identified the N-terminus of β_4 as a possible determinant of nuclear accumulation. In support with the previous hypothesis, our own results show that this domain only partially interferes with β_4 nuclear accumulation suggesting the existence of different pathways controlling β_4 subcellular localization involving different β_4 protein partners. We demonstrate here that the N-terminus of β_4 is not important for its interaction with B56δ suggesting that its contribution to nuclear accumulation occurs through a B56δ-independent pathway. In our work, we focused on the β_4 nuclear pathway that involves B56d and that is disrupted by the human epileptic mutation of β_4. We show that *in vitro* TRα acts as a transcription factor capable to interact with β_4 and repress TH gene expression. The in vivo implication of TRa in controlling TH gene expression remains to be deciphered. The resulting nuclear platform, structured by β_4, binds to specific gene promoters, dephosphorylates histones associated to these promoters and orients HP1γ interaction with the dephosphorylated histones. The formation of this complex allows gene repression, first by a direct effect of β_4 on TRα, and secondly by HP1γ recruitment known to promote heterochromatin formation (Figure 8b). This later step may lead to long-term gene repression, while the first step is conceptually more dynamic. In *lh* brain, a complete disorganization of this signaling pathway is observed in the absence of β_4. The combined reduction in HP1γ levels and greater phosphorylation level of histone H3 Ser^{10}, are two events that conceptually may favor the up-regulation of TH expression. In that respect, further studies on the ability of nuclear β_4 complex to induce other histone post-translational modifications, such as methylation or acetylation, will complete the characterization of the role of this complex in gene regulation. While our data demonstrate the key role of β_4 in organizing TH gene repression, TH expression is not

uniformly up-regulated in all *lh* brain areas indicating the existence of compensatory mechanisms. In that respect, B56γ, that also targets PP2A to the nucleus (McCright et al, 1996), and β_3, another VGCC subunit, that is also addressed to the nucleus (Beguin et al, 2006) and binds B56δ (Figure 4c) and TRα (unpublished observation), might participate to this compensation process. The juvenile epilepsy mutant that normally associates with VGCC (Escayg et al, 2000), is defective for B56δ association. This mutant no longer forms a complex with PP2A, and is unable to translocate to the nucleus and to interact with HP1γ and histones (Figure 8b). Therefore, this mutation induces a full destabilization of the β_4 signaling pathway. At the structural level, formation of the B56δ/β_4 complex requires the interaction between the β_4 SH3 and GK modules. The nuclear targeting defect induced by the human mutation resides in the loss of this interaction highlighting an unexpected role of β_4 C-terminal domain in controlling β_4 conformation state. Association of B56δ with β_4 promotes β_4/HP1γ interaction further indicating the exquisite modularity of β_4 as an adaptor protein.

In earlier reports, B56δ/PP2A was shown to regulate gene expression through a complex interplay between DARPP-32 phosphorylation state (Ahn et al, 2007), phosphatase 1 (PP1) activity, and histone H3 phosphorylation level (Stipanovich et al, 2008). PP1 complexes have been associated to other histone-modifying enzymes, such as histone deacetylases or kinases, with chromatin remodeling capabilities (Hsu et al, 2000; Murnion et al, 2001) and with transcription repressors or activators (Canettieri et al, 2003; Jin et al, 2003). Here, we illustrate that, like PP1, PP2A belongs to a signaling macromolecular complex which ultimately regulates gene expression by modulating the histone code. This complex is organized by the VGCC β_4 subunit that plays the role of a

platform that, besides PP2A, also recruits a nuclear receptor and a heterochromatin protein, HP1γ. By homology with PP1, this protein complex is likely to be enriched by other nucleosome-modifying enzymes in the near future. It should be emphasized that long-term modifications accompanying epileptic disorders have previously been associated to changes in post-translational state of histones and to alterations in transcriptional programs (Huang et al, 2002; Sng et al, 2006). This work thus opens exciting perspectives for understanding the underlying molecular causes of epilepsy in which VGCC subunits have been implicated.

Material and Methods

Mice lines

Lethargic (B6EiC3H-a/A-*lh*) and wild-type mice (strain B6EiC3H) were obtained from Jackson Labs and genotyped as previously described (Burgess et al, 1997). B56$\delta^{-/-}$ mice were generated by exchanging 146 bp of exon 3, exons 4 to 14, and 45 bp of exon 15 of the *Ppp2r5d* gene with a neomycine cassette through homologous recombination (Louis et al, 2011). Animal procedures were run with the approval of the local ethical committee and all efforts were made to minimize both the suffering and number of animal used. Also, the experiments were carried out in accordance with the International Ethical Committee Guidelines (EEC Council Directive 86/609, OJ L 358, 1, Dec. 12, 1987; Guide for the Care and Use of Laboratory Animals, U.S. National Research Council, 1996) for the care and use of laboratory animals.

Electron microscopy

Mice were fixed by intracardiac perfusion during 10 minutes with 50 ml of fixation buffer (2% paraformaldehyde, 0.2% glutaraldehyde in 0.1 M phosphate buffer pH 7.3). The hippocampus was then isolated and kept in fixation buffer during 2 days. A transversal slice was made in the mid third of the hippocampus and dissection of the CA1/CA3 area in this slice was performed under a binocular magnifier. Hippocampal neurons were cultured in B100 plates during 5 or 18 days and fixed 2 hrs with fixation buffer. Cells were gently detached with a cell scraper, centrifuged and embedded in 10% gelatine. The cell pellet was then cut in small pieces. 1 mm^3 cell or tissue samples were then incubated during 4 hrs in 2.3 M sucrose and frozen in liquid nitrogen. Cryosections were made at -120°C using a cryo-ultramicrotome (Leica-Reichert) and retrieved with a 1:1 solution of 2.3 M sucrose and 2% methylcellulose (Liou et al, 1996). Cryosections were first incubated with primary anti-β_4 (Everest Biotech, 1:100), then incubated with rabbit anti-goat antibodies (Jackson, 1:400) and revealed with protein A-gold conjugated (CMC, Utrecht). Labelled cryosections were viewed at 80 kV with a 1200EX JEOL TEM microscope and images were acquired with a digital camera (Veleta, SIS, Olympus). Gold particles were counted and surface area measured with iTEM software (analySIS).

Hippocampal neurons, NG108-15 cell cultures and cerebellar granule neurons

Primary cultures of hippocampal neurons were prepared as previously described (Peris et al, 2009). Astrocyte proliferation was blocked by 10 μM arabinoside cytosine (AraC) four days after plating. Predominance of neurons was witnessed by Tuj1 labeling and lack of GFAP staining. NG108.15 cells were differentiated two days after plating by decreasing fetal calf serum to 1% and addition of 1 mM dibutyryl cAMP. Cell lines were

transfected using jetPEI and neurons at 9 DIV using calcium phosphate. Dissociated cerebellar granule neurons were prepared as previously described (Kiyonaka et al, 2007) except that 0.02% (w/v) trypsin (Difco) was used for dissociation of cerebellar tissues. Three hrs after cell plating, culture medium was replaced with Neurobasal (Invitrogen) with 2% B-27 (GIBCO), 26 mM KCl, 60 U/ml penicillin, and 60 μg/ml streptomycin, and renewed every 3 days. At 8 DIV, 0.1 μM TTX was added in the culture medium to block electrical activity. At 9 DIV, the TTX was washed out to promote electrical activity or maintained for continued electrical activity block. At 10 DIV, total RNA was isolated using NucleoSpin RNA XS (Macherey-Nagel) according to the manufacturer's instructions.

Plasmid constructions

cDNA constructs coding for EGFP-tagged β_4 fragments were generated by PCR amplification using rat β_4-EGFP plasmid as template (Genbank accession code L02315) and subcloned into pEGFP-C1 using *Hind*III and *Kpn*I sites. Myc-tagged β_4 fragments were subcloned into pcDNA3.1(+) using *Hind*III and *Xba*I sites. For yeast two-hybrid assays, rat β_1, β_2, β_3, β_4, and β_4 mutants were subcloned into pGBK-T7 vector(Kiyonaka et al, 2007). QuikChange® Site-Directed Mutagenesis Kit (Stratagene) or overlap extension method was used to produce β_{L125P}-EGFP, β_{P225R}-EGFP, $\beta_{1\text{-}166\text{-}L125P}$-EGFP, $\beta_{P220A\text{-}V222A}$-myc and $\beta_{R28A\text{-}R29A\text{-}S30A}$-EGFP. Mouse B56δ (Genbank accession code NM009358), HP1γ (NM_007624) and TRα (NM_178060) were cloned from mouse brain Marathon-Ready cDNA (Clontech) using PCR and inserted into pCMV-tag3 vector and pEGFP-C2 vector using *Eco*RI and *Sal*I site. The B56δ and control shRNAs (sense

strand sequences: 5'-CATCGCATCTATGGCAAGTTT-3' and 5'-CAACAAGATGAAGAGCACCAA-3', respectively) were subcloned in TRC1.5 vector (Sigma). All constructs were sequenced. Human Cacna1a (Genbank accession code AF004883) and rat Cacna1a (code NM012919) were also used for expression experiments. The TH-luciferase reporter gene was as previously described (Robert et al, 1997) and contains 5,200 bps of the TH promoter upstream of the *Firefly* luciferase coding region.

Cytochemical stainings

Cells were fixed with 4% paraformaldehyde in PBS for 15 min. After PBS washing, plasma membranes were stained 5 min with 5 µg/ml concanavalin A-rhodamine. Cells were permeabilized with 0.1% Triton X-100. Myc-tagged constructs were visualized using biotinylated anti-myc antibodies (1:600, Santa Cruz) and Cy3-Streptavidin (1:300, Amersham). Endogenous β_4 was labeled for 1-2 hrs with a goat antibody directed against its carboxyl-terminus (1/1,000 dilution, Everest Biotech), followed by Alexa488 conjugated anti-goat (1:500, Molecular Probes). Cell nuclei were visualized using ToPro3 dye (T3605; Molecular Probes Inc). Images were obtained with a confocal microscope (Leica SP2). NCR values correspond to the average measure of 50 cells. In each cell, fluorescence intensities were measured in forty different ROI (20 for the cytoplasm and 20 for the nucleus). Merged pictures were obtained by using Adobe Photoshop software.

Yeast two hybrid assays

Rat β_4, subcloned into pGBK-T7, was used as bait to screen a mouse brain pACT2 library expressed in the yeast strain AH109 (Clontech) (Kiyonaka et al, 2007). 5.0 x 10^6

transformants were cultured with synthetic medium lacking adenine, histidine, leucine, and tryptophan. His^+ colonies were assayed in yeast cells for β-galactosidase activity by a filter assay. Signal strengths of interactions were evaluated visually after every 1 hr of color development. For mapping of the β_4 region that interacts with B56δ or HP1γ, yeast strain Y187 was co-transformed with each β bait vector and the B56δ or HP1γ prey vector. The interactions were evaluated by β-galactosidase activity on a filter.

Subcellular fractionation and Western blotting

Transfected HEK293 cells were lysed with 10 mM Tris pH 7.5, 10 mM KCl, 1.5 mM $MgCl_2$, 0.5% Triton X-100 and protease inhibitor cocktail (Roche). Nuclei and cytoplasm were separated by 5 min centrifugation at 2,000 rpm. Pellets corresponding to nuclei were sonicated in lysis buffer. For mice brain subcellular fractionation, brains were homogeneized in 0.32 M sucrose, 20 mM HEPES, pH 7.4, 1 mM DTT, 1 mM PMSF and protease inhibitor cocktail (Roche). The homogeneate was centrifuged 10 min at 800×g. The resulting crude nuclear pellet was washed twice with homogeneization buffer, resuspended in a volume equivalent to the cytoplasmic fraction, and sonicated. Nuclear and cytoplasmic (supernatant) proteins, from equal volumes, were separated by SDS-PAGE and analyzed by Western blot. EGFP tagged-proteins were visualized using anti-EGFP antibodies (1:300, Santa Cruz or 1:5,000 Rockland) and anti-β_4 as described (Kiyonaka et al, 2007).

Immunoprecipitation experiments

Transfected cells were lysed 30 min in 10 mM Tris pH 7.4, 1.5 mM $MgCl_2$, 60 mM KCl, 15 mM NaCl, 0.5% Triton X-100 supplemented with protease inhibitor cocktail (Roche), sonicated and centrifuged 5 min at 1,500×g. Similar procedure applies for mice brain, except that they were homogeneized first in lysis buffer. Protein extracts were incubated with streptavidin beads (Dynabeads® Streptavidin M-280, Dynal) precoated with 3 μg of biotinylated anti-myc antibody (Santa Cruz Biotechnology Inc.). For immunoprecipitation of endogenous β_4, protein extracts were incubated with 40 μl of dynabeads® protein G (Dynal) precoated with anti-β_4 antibodies (Everest Biotech). Beads were washed with PBS/0.1% Tween 20. Immunoprecipitated proteins were eluted with denaturating buffer and analyzed by Western blot. For immunoprecipitation of phosphorylated histones, lysis buffer was supplemented with 50 mM NaF phosphatase inhibitor. For immunoprecipitation and ChIP, primary antibodies were used at 10 μg: anti-β_4 from Everest or as described (Kiyonaka et al, 2007), anti-histone H2B from Upstate, anti-histone H3, anti-phosphorylated Ser^{10} histone H3, anti-histone H4, anti-HP1γ, and anti-TRα from Abcam, anti-B56δ as described in(Martens et al, 2004), anti-PP2A from Bethyl laboratories Inc., and anti-actin from Sigma-Aldrich.

PP2A activity

PP2A activity of immunoprecipitates was measured using SensoLyte™*p*NPP protein phosphatase kit from AnaSpec. Incubation lasted 1 hr at 37°C in assay buffer in the presence of *p*-nitrophenyl phosphate (pNPP). OD was measured at 405 nm.

Quantitative RT-PCR

Total RNAs were extracted from wt, *lh* or B56δ$^{-/-}$ cerebellum using the RNeasy kit, supplemented with DNase I (Qiagen). cDNAs were synthesized from 1 µg total RNA using random hexamer primers (Promega) and Superscript II (Invitrogen). Primers recognizing mice sequences were designed with the Primer 3 software (http://frodo.wi.mit.edu/) or by Sigma service (Supplementary Figure 10). Real time PCR was performed with a light cycler 480 instrument using the Lightcycler LC480 SYBR green I master (Roche) according to the manufacturer's instructions. The cycling protocol was 10 min at 95°C followed by 40 cycles of 3 steps each (10 sec at 95°C, 5 sec at 60°C, and 10 sec at 72°C). The specificity of the amplification was check by generating a melting curve ranging from 65 to 95°C. Multiple normalization of gene expression (Vandesompele et al, 2002) was performed using 3 housekeeping genes (glyceraldehyde 3-phosphate dehydrogenase, transferin receptor, and peptidylprolyl isomerase A).

For TH expression levels in cerebellar granule neurons, cDNAs were synthesized using AMV reverse transcriptase XL and an oligo dT-adaptor primer (TaKaRa). Real time PCR and cycling protocol were performed as above, except for the number of cycles (50). TH gene expression was normalized relative to rpl27 (de Jonge et al, 2007). Values were expressed relative to wt treated with TTX, which was given the arbitrary value of 1.

Chromatin immunoprecipitation

Frozen adult mice brain (wt, *lh* or B56δ$^{-/-}$) brain were first crunched into powder in a mortar filled with liquid nitrogen. This powder was resuspended in 1% formaldehyde (in PBS) and incubated for 20 min at RT. Cross linking was stopped by addition of glycine (125 mM final concentration) and incubation 5 min. Fixed tissues were thus washed with

i) cold PBS (5 min), ii) 10 mM HEPES, 0.5 mM EGTA, 10 mM EDTA and Triton X-100 0.25%, pH 7.4 (10 min), and iii) 10 mM HEPES, 0.5 mM EGTA, 1 mM EDTA and 200 mM NaCl, pH 7.4 (10 min). Samples were then solubilized in 1 ml of buffer containing 50 mM Tris, pH 7.4, 10 mM EDTA, 1% SDS for 2 hrs at 4°C, sonicated until reaching an average 500-1,000 bps DNA fragment size, and centrifuged 5 min at 20,000 g. 100 µl of lysate (DO_{280} = 0.266) were incubated overnight at 4°C in 1 ml of 0.01% SDS, 1.1% Triton X100, 1.2 mM EDTA, 16 mM Tris pH 8.0 and 170 mM NaCl, 1 mM PMSF, and protease inhibitor cocktail, with or without 10 µg antibodies. Immunoprecipitation was performed by adding dynabeads protein G (Invitrogen). Different washing steps and elution were performed as described (Dahl & Collas, 2008). Cross-links were reversed overnight at 65°C. DNA samples were sequentially treated with RNAse A and proteinase K. DNA was extracted by phenol/chloroform and ethanol precipitated with glycogen as a carrier. DNA pellet was dissolved in water and real-time quantitative PCR analyses were performed on 25 ng of DNA in duplicate with selected primers (Supplementary Figure 10). On cultured hippocampal neurons, ChIP experiments were conducted on 5×10^6 cells using the Magna ChIP™ (MILLIPORE) according to the manufacture's protocol. The PCR cycling protocol was 10 min at 94°C followed by 38 cycles of 3 steps each (30 sec at 94°C, 30 sec at 55°C or 61°C, and 30 sec at 72°C), and 7 min at 72°C. Annealing temperature for the promoter region of TH was 55°C and for the 3'UTR of TH was 61°C.

Mass spectrometry

The histone H3 peptide phosphorylated at Ser^{10} $QTARKS_pTGGC$ was obtained from Smartox biotechnologies (Grenoble, France). Immunoprecipitates were washed with (in

mM) 40 Tris pH 8.4, 34 $MgCl_2$, 4 EDTA, 4 DTT, and incubated overnight at 37°C with 1 mM peptide. Dephosphorylation was evaluated by MALDI-TOF (Applied 4800) mass spectrometry. Briefly, 1 µl of peptide solution was spotted directly onto the MALDI target, dried and 1 µl of 20% α-Cyano-4-hydroxy-cinnamic acid (Sigma) was added in 50% acetonitril, 0.1% trifluoracetic acid.

Acknowledgments

We are indebted to Dr. Hiroshi Hibino (Osaka University, Japan) for providing HP1γ constructs used for coimmunoprecipitation, confocal imaging and yeast two hybrid assays. We thank Dr. Rosalie Sears (Oregon Health & Sciences University, Portland, USA) for the pD30-PP2A-HA-C clone. M.B. is a postdoctoral fellow of Association Française contre les Myopathies. The authors declare that they have no conflict of interest.

Author contributions: A.T. and K.F. studied the nuclear localization of β_4 and its structural determinants. Sh.K., T.M., S.A. made several cDNA constructs and performed yeast two-hybrid and ChIP experiments. M.B., K.F. and Mi.R. performed RT-PCR, immunoprecipitation and ChIP experiments. C.A. did electrophysiological recordings. S.G-F. and A.A. provided their expertise with hippocampal neuron cultures. K.S. performed mass spectrometry experiments and Sa.K. contributed to discussion, design and interpretation of data regarding nuclear function of β_4 complex. F.L. performed CHCB2 experiments. K.P-G. did EM experiments. S.B. performed transcriptomic analyses. C.L. and V.J. provided the B56$\delta^{-/-}$ mice line and analytical tools. R.D., Mi.R., Y.M. and M.D.W. coordinated the study. Mi.R. and M.D.W. wrote the manuscript.

Conflict of interest

The authors declare that they have no conflict of interest.

References

Ahn JH, McAvoy T, Rakhilin SV, Nishi A, Greengard P, Nairn AC (2007) Protein kinase A activates protein phosphatase 2A by phosphorylation of the B56delta subunit. *Proc Natl Acad Sci U S A* **104**(8)**:** 2979-2984

Arikkath J, Campbell KP (2003) Auxiliary subunits: essential components of the voltage-gated calcium channel complex. *Curr Opin Neurobiol* **13**(3)**:** 298-307

Beguin P, Mahalakshmi RN, Nagashima K, Cher DH, Ikeda H, Yamada Y, Seino Y, Hunziker W (2006) Nuclear sequestration of beta-subunits by Rad and Rem is controlled by 14-3-3 and calmodulin and reveals a novel mechanism for Ca2+ channel regulation. *J Mol Biol* **355**(1)**:** 34-46

Bengzon J, Hansson SR, Hoffman BJ, Lindvall O (1999) Regulation of norepinephrine transporter and tyrosine hydroxylase mRNAs after kainic acid-induced seizures. *Brain Res* **842**(1)**:** 239-242

Bichet D, Cornet V, Geib S, Carlier E, Volsen S, Hoshi T, Mori Y, De Waard M (2000) The I-II loop of the Ca2+ channel alpha1 subunit contains an endoplasmic reticulum retention signal antagonized by the beta subunit. *Neuron* **25**(1)**:** 177-190

Bidaud I, Mezghrani A, Swayne LA, Monteil A, Lory P (2006) Voltage-gated calcium channels in genetic diseases. *Biochim Biophys Acta* **1763**(11)**:** 1169-1174

Burgess DL, Jones JM, Meisler MH, Noebels JL (1997) Mutation of the Ca2+ channel beta subunit gene Cchb4 is associated with ataxia and seizures in the lethargic (lh) mouse. *Cell* **88**(3)**:** 385-392

Canettieri G, Morantte I, Guzman E, Asahara H, Herzig S, Anderson SD, Yates JR, 3rd, Montminy M (2003) Attenuation of a phosphorylation-dependent activator by an HDAC-PP1 complex. *Nat Struct Biol* **10**(3)**:** 175-181

Carrion AM, Link WA, Ledo F, Mellstrom B, Naranjo JR (1999) DREAM is a Ca2+-regulated transcriptional repressor. *Nature* **398**(6722)**:** 80-84

Catterall WA, Perez-Reyes E, Snutch TP, Striessnig J (2005) International Union of Pharmacology. XLVIII. Nomenclature and structure-function relationships of voltage-gated calcium channels. *Pharmacol Rev* **57**(4)**:** 411-425

Chemin J, Nargeot J, Lory P (2002) Neuronal T-type alpha 1H calcium channels induce neuritogenesis and expression of high-voltage-activated calcium channels in the NG108-15 cell line. *J Neurosci* **22**(16)**:** 6856-6862

Chen YH, Li MH, Zhang Y, He LL, Yamada Y, Fitzmaurice A, Shen Y, Zhang H, Tong L, Yang J (2004) Structural basis of the alpha(1)-beta subunit interaction of voltage-gated Ca(2+) channels. *Nature* **429**(6992)**:** 675-680

Dahl JA, Collas P (2008) A rapid micro chromatin immunoprecipitation assay (microChIP). *Nat Protoc* **3**(6)**:** 1032-1045

de Jonge HJ, Fehrmann RS, de Bont ES, Hofstra RM, Gerbens F, Kamps WA, de Vries EG, van der Zee AG, te Meerman GJ, ter Elst A (2007) Evidence based selection of housekeeping genes. *PLoS One* **2**(9)**:** e898

Deisseroth K, Mermelstein PG, Xia H, Tsien RW (2003) Signaling from synapse to nucleus: the logic behind the mechanisms. *Curr Opin Neurobiol* **13**(3)**:** 354-365

Dolmetsch RE, Pajvani U, Fife K, Spotts JM, Greenberg ME (2001) Signaling to the nucleus by an L-type calcium channel-calmodulin complex through the MAP kinase pathway. *Science* **294**(5541)**:** 333-339

Donato R, Page KM, Koch D, Nieto-Rostro M, Foucault I, Davies A, Wilkinson T, Rees M, Edwards FA, Dolphin AC (2006) The ducky(2J) mutation in Cacna2d2 results in reduced spontaneous Purkinje cell activity and altered gene expression. *J Neurosci* **26**(48)**:** 12576-12586

Escayg A, De Waard M, Lee DD, Bichet D, Wolf P, Mayer T, Johnston J, Baloh R, Sander T, Meisler MH (2000) Coding and noncoding variation of the human calcium-channel beta4-subunit gene CACNB4 in patients with idiopathic generalized epilepsy and episodic ataxia. *Am J Hum Genet* **66**(5)**:** 1531-1539

Fischle W, Tseng BS, Dormann HL, Ueberheide BM, Garcia BA, Shabanowitz J, Hunt DF, Funabiki H, Allis CD (2005) Regulation of HP1-chromatin binding by histone H3 methylation and phosphorylation. *Nature* **438**(7071)**:** 1116-1122

Flavell SW, Greenberg ME (2008) Signaling mechanisms linking neuronal activity to gene expression and plasticity of the nervous system. *Annu Rev Neurosci* **31:** 563-590

Gomez-Ospina N, Tsuruta F, Barreto-Chang O, Hu L, Dolmetsch R (2006) The C terminus of the L-type voltage-gated calcium channel Ca(V)1.2 encodes a transcription factor. *Cell* **127**(3)**:** 591-606

Graef IA, Mermelstein PG, Stankunas K, Neilson JR, Deisseroth K, Tsien RW, Crabtree GR (1999) L-type calcium channels and GSK-3 regulate the activity of NF-ATc4 in hippocampal neurons. *Nature* **401**(6754)**:** 703-708

Greer PL, Greenberg ME (2008) From synapse to nucleus: calcium-dependent gene transcription in the control of synapse development and function. *Neuron* **59**(6)**:** 846-860

Hardingham GE, Arnold FJ, Bading H (2001) Nuclear calcium signaling controls CREB-mediated gene expression triggered by synaptic activity. *Nat Neurosci* **4**(3)**:** 261-267

Hardingham GE, Chawla S, Johnson CM, Bading H (1997) Distinct functions of nuclear and cytoplasmic calcium in the control of gene expression. *Nature* **385**(6613)**:** 260-265

Hess EJ, Wilson MC (1991) Tottering and leaner mutations perturb transient developmental expression of tyrosine hydroxylase in embryologically distinct Purkinje cells. *Neuron* **6**(1)**:** 123-132

Hibino H, Pironkova R, Onwumere O, Rousset M, Charnet P, Hudspeth AJ, Lesage F (2003) Direct interaction with a nuclear protein and regulation of gene silencing by a variant of the Ca2+-channel beta 4 subunit. *Proc Natl Acad Sci U S A* **100**(1)**:** 307-312

Hsu JY, Sun ZW, Li X, Reuben M, Tatchell K, Bishop DK, Grushcow JM, Brame CJ, Caldwell JA, Hunt DF, Lin R, Smith MM, Allis CD (2000) Mitotic phosphorylation of histone H3 is governed by Ipl1/aurora kinase and Glc7/PP1 phosphatase in budding yeast and nematodes. *Cell* **102**(3)**:** 279-291

Huang Y, Doherty JJ, Dingledine R (2002) Altered histone acetylation at glutamate receptor 2 and brain-derived neurotrophic factor genes is an early event triggered by status epilepticus. *J Neurosci* **22**(19)**:** 8422-8428

Jenuwein T, Allis CD (2001) Translating the histone code. *Science* **293**(5532)**:** 1074-1080

Jin Q, van Eynde A, Beullens M, Roy N, Thiel G, Stalmans W, Bollen M (2003) The protein phosphatase-1 (PP1) regulator, nuclear inhibitor of PP1 (NIPP1), interacts with the polycomb group protein, embryonic ectoderm development (EED), and functions as a transcriptional repressor. *J Biol Chem* **278**(33)**:** 30677-30685

Kiyonaka S, Wakamori M, Miki T, Uriu Y, Nonaka M, Bito H, Beedle AM, Mori E, Hara Y, De Waard M, Kanagawa M, Itakura M, Takahashi M, Campbell KP, Mori Y (2007) RIM1 confers sustained activity and neurotransmitter vesicle anchoring to presynaptic Ca2+ channels. *Nat Neurosci* **10**(6)**:** 691-701

Liou W, Geuze HJ, Slot JW (1996) Improving structural integrity of cryosections for immunogold labeling. *Histochem Cell Biol* **106**(1)**:** 41-58

Louis JV, Martens E, Borghgraef P, Lambrecht C, Sents W, Longin S, Zwaenepoel K, Pijnenborg R, Landrieu I, Lippens G, Ledermann B, Gotz J, Van Leuven F, Goris J, Janssens V (2011) Mice lacking phosphatase PP2A subunit PR61/B'delta (Ppp2r5d) develop spatially restricted tauopathy by deregulation of CDK5 and GSK3beta. *Proc Natl Acad Sci U S A* **108**(17)**:** 6957-6962

Magnusdottir A, Stenmark P, Flodin S, Nyman T, Kotenyova T, Graslund S, Ogg D, Nordlund P (2009) The structure of the PP2A regulatory subunit B56 gamma: the remaining piece of the PP2A jigsaw puzzle. *Proteins* **74**(1)**:** 212-221

Martens E, Stevens I, Janssens V, Vermeesch J, Gotz J, Goris J, Van Hoof C (2004) Genomic organisation, chromosomal localisation tissue distribution and developmental regulation of the PR61/B' regulatory subunits of protein phosphatase 2A in mice. *J Mol Biol* **336**(4)**:** 971-986

McCright B, Rivers AM, Audlin S, Virshup DM (1996) The B56 family of protein phosphatase 2A (PP2A) regulatory subunits encodes differentiation-induced phosphoproteins that target PP2A to both nucleus and cytoplasm. *J Biol Chem* **271**(36)**:** 22081-22089

McGee AW, Nunziato DA, Maltez JM, Prehoda KE, Pitt GS, Bredt DS (2004) Calcium channel function regulated by the SH3-GK module in beta subunits. *Neuron* **42**(1)**:** 89-99

Murnion ME, Adams RR, Callister DM, Allis CD, Earnshaw WC, Swedlow JR (2001) Chromatin-associated protein phosphatase 1 regulates aurora-B and histone H3 phosphorylation. *J Biol Chem* **276**(28)**:** 26656-26665

Nowak SJ, Pai CY, Corces VG (2003) Protein phosphatase 2A activity affects histone H3 phosphorylation and transcription in Drosophila melanogaster. *Mol Cell Biol* **23**(17)**:** 6129-6138

Oliveria SF, Dell'Acqua ML, Sather WA (2007) AKAP79/150 anchoring of calcineurin controls neuronal L-type Ca2+ channel activity and nuclear signaling. *Neuron* **55**(2)**:** 261-275

Peris L, Wagenbach M, Lafanechere L, Brocard J, Moore AT, Kozielski F, Job D, Wordeman L, Andrieux A (2009) Motor-dependent microtubule disassembly driven by tubulin tyrosination. *J Cell Biol* **185**(7)**:** 1159-1166

Restituito S, Cens T, Rousset M, Charnet P (2001) Ca(2+) channel inactivation heterogeneity reveals physiological unbinding of auxiliary beta subunits. *Biophys J* **81**(1)**:** 89-96

Robert JJ, Geoffroy MC, Finiels F, Mallet J (1997) An adenoviral vector-based system to study neuronal gene expression: analysis of the rat tyrosine hydroxylase promoter in cultured neurons. *J Neurochem* **68**(5)**:** 2152-2160

Rosen LB, Ginty DD, Weber MJ, Greenberg ME (1994) Membrane depolarization and calcium influx stimulate MEK and MAP kinase via activation of Ras. *Neuron* **12**(6)**:** 1207-1221

Sandoz G, Lopez-Gonzalez I, Grunwald D, Bichet D, Altafaj X, Weiss N, Ronjat M, Dupuis A, De Waard M (2004) Cavbeta-subunit displacement is a key step to induce the reluctant state of P/Q calcium channels by direct G protein regulation. *Proc Natl Acad Sci U S A* **101**(16)**:** 6267-6272

Sng JC, Taniura H, Yoneda Y (2006) Histone modifications in kainate-induced status epilepticus. *Eur J Neurosci* **23**(5)**:** 1269-1282

Spafford JD, Van Minnen J, Larsen P, Smit AB, Syed NI, Zamponi GW (2004) Uncoupling of calcium channel alpha1 and beta subunits in developing neurons. *J Biol Chem* **279**(39)**:** 41157-41167

Stipanovich A, Valjent E, Matamales M, Nishi A, Ahn JH, Maroteaux M, Bertran-Gonzalez J, Brami-Cherrier K, Enslen H, Corbille AG, Filhol O, Nairn AC, Greengard P, Herve D, Girault JA (2008) A phosphatase cascade by which rewarding stimuli control nucleosomal response. *Nature* **453**(7197)**:** 879-884

Subramanyam P, Obermair GJ, Baumgartner S, Gebhart M, Striessnig J, Kaufmann WA, Geley S, Flucher BE (2009) Activity and calcium regulate nuclear targeting of the calcium channel beta(4b) subunit in nerve and muscle cells. *Channels (Austin)* **3**(5)**:** 343-355

Takahashi SX, Miriyala J, Colecraft HM (2004) Membrane-associated guanylate kinase-like properties of beta-subunits required for modulation of voltage-dependent Ca2+ channels. *Proc Natl Acad Sci U S A* **101**(18)**:** 7193-7198

Takahashi SX, Miriyala J, Tay LH, Yue DT, Colecraft HM (2005) A CaVbeta SH3/guanylate kinase domain interaction regulates multiple properties of voltage-gated Ca2+ channels. *J Gen Physiol* **126**(4)**:** 365-377

Vandesompele J, De Preter K, Pattyn F, Poppe B, Van Roy N, De Paepe A, Speleman F (2002) Accurate normalization of real-time quantitative RT-PCR data by geometric averaging of multiple internal control genes. *Genome Biol* **3**(7)**:** 34

Xu X, Lee YJ, Holm JB, Terry MD, Oswald RE, Horne WA (2011) The Ca2+ channel beta4c subunit interacts with heterochromatin protein 1 via a PXVXL binding motif. *J Biol Chem* **286**(11)**:** 9677-9687

Figure legends

Figure 1 Presence of β_4 in the nucleus of neurons. (**a**) Immunohistochemical confocal images of 20 µm coronal sections of adult wt (upper panels) or *lh* (lower panels) mice brains showing the distribution of endogenous β_4 in the dentate gyrus (green, left panels). Neuronal nuclei were labeled with NeuN (blue, middle panels). Right panels illustrate merged images. The inserts show 5X images of the CA3 region (initially 20X). (**b**) Western blots of adult wt and *lh* mice brain lysates indicating the presence of β_4 only in wt mice. Actin staining was used as an internal control. (**c**) β_4 immunoblotting from cytoplasmic and nuclear fractions of adult wt mice brain. β-tubulin and nucleolin are used as indicators of nuclear and cytoplasmic fraction purities, respectively. (**d**) EM image of an ultrathin cryosection of the CA1 hippocampal region showing the intranuclear presence of β_4 labelled with antibody-coated 15 nm gold particles. Black and white arrows indicate the position of gold particles associated to heterochromatin and euchromatin, respectively. (**e**) Confocal images of hippocampal neurons from embryonic E18 mice brains in primary culture at 5 DIV (left panels) and 18 DIV (right panels). Green: immunocytochemical staining of β_4; red: membrane staining with concanavalin A (ConA) conjugated to rhodamine; blue: nuclear staining with ToPro3. (**f**) DIV-dependent evolution of β_4 NCR values in neurons (n=50 cells for each data point). (**g**) Nuclear density of β_4 in hippocampal neurons at 5 and 18 DIV as assessed by EM (n=28 and 20 nuclei, respectively). (**h**) Confocal images of NG108.15 cells 1 day before (-1 DIV) and 13 days (13 DIV) after induction of neuronal differentiation with 1 mM cAMP and serum

reduction. Color code is as in (**e**). Differentiated NG108-15 cells have larger nuclei than non-differentiated cells. (**i**) Mean NCR values expressed in percent as a function of culture time *in vitro*. DIV 0 represents the induction time of neuronal differentiation.

Figure 2 Nuclear targeting and structural integrity of β_4 are disrupted by the human juvenile epilepsy mutation. (**a**) Schematic representation of different truncated β_4 constructs in pEGFP-C1. The $\beta_{1\text{-}481}$-EGFP mutant is also shown. (**b**) Confocal images of CHO cells expressing some representative constructs, including β_4-EGFP and mutant $\beta_{1\text{-}481}$-EGFP. Expression time is 24 hrs after transfection. (**c**) Mean NCR values of EGFP fluorescence for each condition in transfected CHO cells. ***, $p \leq 0.01$. (**d**) Western blot detecting EGFP in nuclear and cytoplasmic fractions of CHO cells after two days of transfection with EGFP, β_4-EGFP or $\beta_{1\text{-}481}$-EGFP. Cytoplasmic $\beta_{1\text{-}481}$-EGFP is less stable than cytoplasmic β_4-EGFP, as witnessed by the presence of lower molecular weight bands. These truncated constructs are deficient in nuclear accumulation as shown in (**c**), possibly because containing GK domains. (**e**) Confocal images of hippocampal neurones transfected at 7 DIV with $\beta_{1\text{-}481}$-EGFP (upper panels) or β_4-EGFP (lower panels). Images were acquired at 9 DIV on β-tubulin III-positive cells. (**f**) NCR values for each construct. ***, $p \leq 0.01$. (**g**) Confocal images of hippocampal neurons transfected with $\beta_{1\text{-}481}$-EGFP showing the comparative distribution of endogenous β_4 (red) and exogenous $\beta_{1\text{-}481}$-EGFP (green).

Figure 3 The SH3/GK interaction is required for β_4 nuclear localization. (**a**) EGFP- or myc-tagged β_4-truncated constructs used for confocal microscopy and co-

immunoprecipitation experiments. (**b**) Confocal images of CHO cells transfected with individual constructs. (**c**) Confocal images of CHO cells expressing $\beta_{1\text{-}166}$-EGFP with $\beta_{200\text{-}519}$-myc, or $\beta_{1\text{-}166}$-EGFP with $\beta_{200\text{-}481}$-myc (upper panels). Mean NCR values of EGFP or anti-myc fluorescence summarizing the effect of the co-expressions on nuclear localization (lower panels). ***, $p \leq 0.001$. (**d**) Immunoprecipation experiments in CHO cells investigating the association of $\beta_{1\text{-}166}$-EGFP with $\beta_{200\text{-}519}$-myc or $\beta_{200\text{-}481}$-myc. Left panel: immunoprecipitation via anti-myc antibodies and Western blot of EGFP, except first lane showing β_4-EGFP expression level in cell lysates. Right panel: Western blot with polyclonal anti-β antibody (Bichet et al, 2000) indicating equivalent $\beta_{200\text{-}519}$-myc and $\beta_{200\text{-}481}$-myc immunoprecipitation levels. $\beta_{1\text{-}166}$-EGFP expression confirmed by cell EGFP fluorescence. (**e**) Schematic representation of β_{L125P}-EGFP, $\beta_{1\text{-}166\text{-}L125P}$-EGFP and β_{P225R}-EGFP mutants. (**f**) Lack of co-immunoprecipation shows the absence of $\beta_{200\text{-}519}$-myc/$\beta_{1\text{-}166\text{-}L125P}$-EGFP interaction. Expression of $\beta_{1\text{-}166}$-EGFP and $\beta_{200\text{-}519}$-myc was verified by the cell fluorescence and Western blot as in (**d**). (**g**) Confocal images of hippocampal neurons showing the cytoplasmic localization of β_{L125P}-EGFP and β_{P225R}-EGFP. Cells were transfected for 48 hrs at 6 DIV. (**h**) Mean NCR values for β_4-EGFP, β_{L125P}-EGFP and β_{P225R}-EGFP fluorescence in hippocampal neurons. ***, $p \leq 0.001$.

Figure 4 B56δ/β_4 interaction contributes to β_4 nuclear localization. (**a**) Yeast two hybrid results indicating the interaction level of β_4 and $\beta_{1\text{-}481}$ with B56δ as a function of time (left). The interactions were scored as the ratio of β-galactosidase activity to His prototrophy. Schematic representation of mouse B56δ showing the NLS amino acid

sequence (right). The position of seven HEAT repeats are shown by homology with B56γ (Magnusdottir et al, 2009). (**b**) Co-immunoprecipation experiments determining the interaction between β_4-EGFP or $\beta_{1\text{-}481}$-EGFP with B56δ-myc in HEK293 cells. Left panel: expression of B56δ-myc was confirmed by Western blot (Mr 69 kDa). Right panel: pull-down with anti-myc antibody, and Western blot with anti-EGFP antibody. (**c**) Interactions of β isoforms with B56δ and HP1γ in yeast two hybrid assay. (**d**) Interactions of truncated and mutated β_4 constructs with B56δ using yeast two hybrid assay. (**e**) Effect of B56δ shRNA and control shRNA on the NCR value of β_4-EGFP in CHO cells. ***, $p \leq 0.001$; NS, $p \geq 0.1$. (**f**) Effect of B56δ shRNA and control shRNA on the nuclear / cytoplasmic distribution of β_4-EGFP in CHO cells, as assessed by WB. Histone H3 and β-tubulin are used as markers of the nucleus (N) and cytoplasm (C), respectively. Performed in duplicate. Average ratios of 4.2 ± 0.32 (β_4-EGFP) and 0.97 ± 0.81 (β_4-EGFP + shRNA B56δ). (**g**) Confocal images showing the cell distribution of endogenous β_4 in undifferentiated NG108.15 cells in the absence or presence of B56δ-myc (left panels). B56δ-myc was transfected 24 hrs before confocal imaging. Panels in green present the endogenous β_4 detected with an anti-β_4. Mean NCR values showing that B56δ-myc induces the redistribution of endogenous β_4 to the nucleus (right panel). ***, $p \leq 0.001$. (**h**) Mean NCR values of endogenous β_4 from wt and B56$\delta^{-/-}$ hippocampal neurons at 11 DIV. ***, $p \leq 0.001$. (**i**) Average immunogold-labeled endogenous β_4 in nuclei from pyramidal neurons from wt and B56$\delta^{-/-}$ mice hippocampus measured by EM (n=36 and 51 nuclei, respectively). ***, $p \leq 0.001$. Control counts in *lh* hippocampus were 0.51 ± 0.36 gold particles/µm².

Figure 5 β_4 association to B56δ/PP2A is inhibited by channel expression and activated by membrane depolarization. (**a**) β_4 immunoprecipitates B56δ and PP2A from wt mice brain but not from *lh* or B56δ$^{-/-}$ mice as shown by Western blots. (**b**) Left panel: immunoprecipitation of endogenous PP2A by B56δ-myc or β_4-myc ± B56δ-EGFP expressed in HEK293 cells. Right panel: similar experiments using $\beta_{1\text{-}481}$-myc ± B56δ-EGFP. (**c**) Endogenous PP2A phosphatase activity associated to immunoprecipitated β_4-myc ± B56δ-EGFP expressed in HEK293 cells. Dephosphorylation of *p*-nitrophenyl phosphate (*p*NPP), a generic phosphatase substrate, was measured by absorbance of the metabolite at 405 nm. Experiment in duplicate. (**d**) Confocal images of HEK293 cells 2 days after transfection with β_4-EGFP together with Cacna1a and Cacna2d2 subunits (VGCC) (left panel). Mean NCR values of EGFP fluorescence in various transfection conditions (n=50 for each condition, right panel). (**e**) Western blot analysis of β_4-EGFP subunit immunoprecipitated by B56δ-myc ± VGCC expressed in HEK293 cells. Control IP represents precipitation in absence of anti-myc antibodies. (**f**) Western blot analysis of B56δ-EGFP immunoprecipitated by β_4-myc (left panels) or $\beta_{1\text{-}481}$-myc (right panels) expressed in HEK293 cells together with VGCC, without or with a 30 min depolarization by 140 mM KCl. (**g**) Effect of HEK293 membrane depolarization (140 mM KCl, 30 min) on β_4-myc or $\beta_{1\text{-}481}$-myc complex formation with PP2A in the presence of B56δ-EGFP and VGCC. (**h**) Mean NCR values of β_4 immunofluorescence in wt or B56δ$^{-/-}$ hippocampal neurons at 18 DIV (control or 1 μM TTX). TTX was added at 11 DIV in the culture media (n=50 for each condition). (**i**) Effect of a 1 hr application of 40 μM

biccuculine and 400 μM 4-AP on average β_4 NCR value in wt and B56$\delta^{-/-}$ hippocampal neurons. NS, non significant; ***, p<0.001.

Figure 6 β_4 regulates gene expression by interacting with a transcription factor. (**a**) Histogram showing up-regulated (in red) and down-regulated (in green) genes displaying a > 2-fold change in *lh versus* wt cerebellum mRNA levels as detected with transcriptomic probe sets. (**b**) qRT-PCR experiments showing up-regulation of TH, TAC1, KLB and down-regulation of BC031748 and RIF1 in *lh versus* wt cerebellum. Mean ± S.D. of 3 experiments performed in triplicate. Data were normalized using 3 housekeeping genes (glyceraldehyde 3-phosphate dehydrogenase, transferin receptor, and peptidylprolyl isomerase A). (**c**) Agarose gel of representative ChIP assay on hippocampal neurons at 1 or 18 DIV with anti-β_4 antibodies. (**d**) TH promoter immunoprecipitation in presence or absence (control) of anti-β_4 antibodies, expressed as percentage of input, from wt or *lh* mice brain (n=4-22, left panel). ***, p<0.001. (**e**) Yeast two hybrid results indicating the interaction level of β_4 with TRα as a function of time (upper panel). The interactions were scored as the ratio of β-galactosidase activity to His prototrophy. Schematic representation of mouse TRα showing the localization of the DNA Binding Domain (DBD) and the Ligand Binding Domain (LBD) (lower panel). (**f**) Western blot analysis of TRα-EGFP immunoprecipitated by β_4-myc expressed in HEK293 cells. (**g**) TH promoter immunoprecipitation by anti-TRα antibodies, expressed as percentage of input, from wt, *lh* or B56$\delta^{-/-}$ mice brain (n=4-20, left panel). ***, p<0.001. (**h**) Schematic representation of the luciferase reporter system under the control of TH promoter (upper panel). Luciferase expression measured in the absence and

presence of T3 in HEK293 cells transfected with the luciferase reporter alone or together with TRα ± β_4 (lower panel). An everted repeat type 6 TRE is present in the promoter region of TH gene (TGGCCTTGCCTGAGGCCA) at position -341 to -323.

Figure 7 Association of β_4 to HP1γ and histones requires B56δ. (**a**) TH promoter immunoprecipitation by anti-B56δ antibodies, expressed as percentage of input, from wt, *lh* or B56δ$^{-/-}$ mice brain (n=2-8). **, $p<0.05$. (**b**) TH promoter immunoprecipitation by anti-PP2A antibodies, expressed as percentage of input, from wt mice brain (n=12). **, $p<0.05$. (**c**) Western blot of H3 and H3 Ser^{10}P in HEK293 cells expressing β_4-myc alone or with B56δ-EGFP. (**d**) Mass spectrometry data showing dephosphorylation of the phosphorylated N-terminal histone H3 peptide (amino acids 5 to 13 phosphorylated on Ser^{10}) by β_4-myc immunoprecipitated from HEK293 cells, cotransfected with B56δ-EGFP and PP2A-HA. (**e**) TH promoter immunoprecipitation by anti-Ser^{10}P H3 or anti-H3 antibodies, expressed as percentage of input, from wt or *lh* mice brain (n=3-22). *, $p<0.1$. (**f**) Schematic representation of β_{4c} and β_4 illustrating the localization of the HP1γ binding motif (critical residues are shadowed). (**g**) Western blot of HP1γ-EGFP following immunoprecipitation by anti-myc antibodies from HEK293 cells expressing various combinations of HP1γ-EGFP, B56δ-EGFP and β_4-myc. (**h**) Immunoprecipitation of histone H3 from wt, *lh* or B56δ$^{-/-}$ brain by anti-β_4 antibodies. (**i**) Immunoprecipitation of H3, H2B and H4 histones from HEK293 cells by β_4-myc in the absence or presence of B56δ-EGFP. Control: immunoprecipitation in non-transfected cells (NT). (**j**) Immunoprecipitation of histone H3 in HEK293 cells by B56δ-myc in the absence or presence of β_4-EGFP. (**k**) Lack of co-immunoprecipitation of histone H4 and B56δ-myc

in HEK293 cells in the presence of β_{L125P}-EGFP or $\beta_{1\text{-}481}$-EGFP mutants. (**l**) TH promoter immunoprecipitation by anti-HP1γ antibodies, expressed as percentage of input, from wt or *lh* mice brain (n=4-14). **, $p<0.05$. (m) Mutation of the HP1γ binding motif prevents β_4-myc association to histone H3 in the presence of B56δ-EGFP.

Figure 8 Experimental validation and schematic illustration of the novel excitation-transcription pathway mediated by β_4. (**a**) Electrical activity reduces TH mRNA levels in primary cultures of cerebellar granule neuronal from wt mice but not *lh* mice. Upper panel represents the experimental protocol. First condition in which TTX is added for 2 days (8 DIV to 10 DIV) is used as control condition without electrical activity (blue colour), whereas second condition in which TTX is washed out at 9 DIV is used as the condition in which electrical activity is restored (red colour). Lower panel illustrates the fold-change in TH mRNA level induced by electrical activity using rpl27 as housekeeping gene and normalisation to control condition. **, $p<0.05$. (**b**) Schematic representation of the new signalling pathway and of the defective steps produced by the epileptic truncation of β_4.

Figure 1 (De Waard)

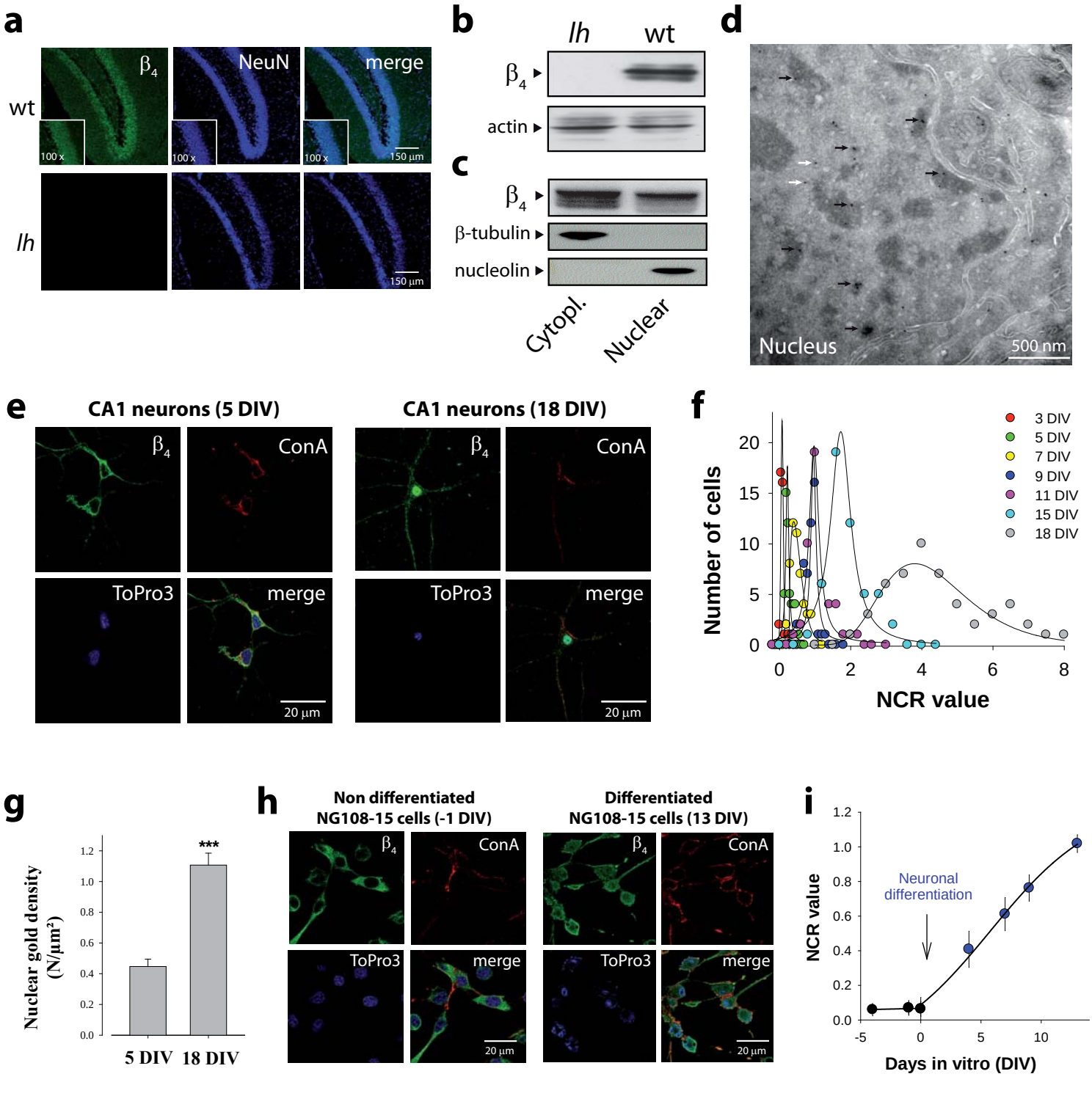

Figure 2 (De Waard)

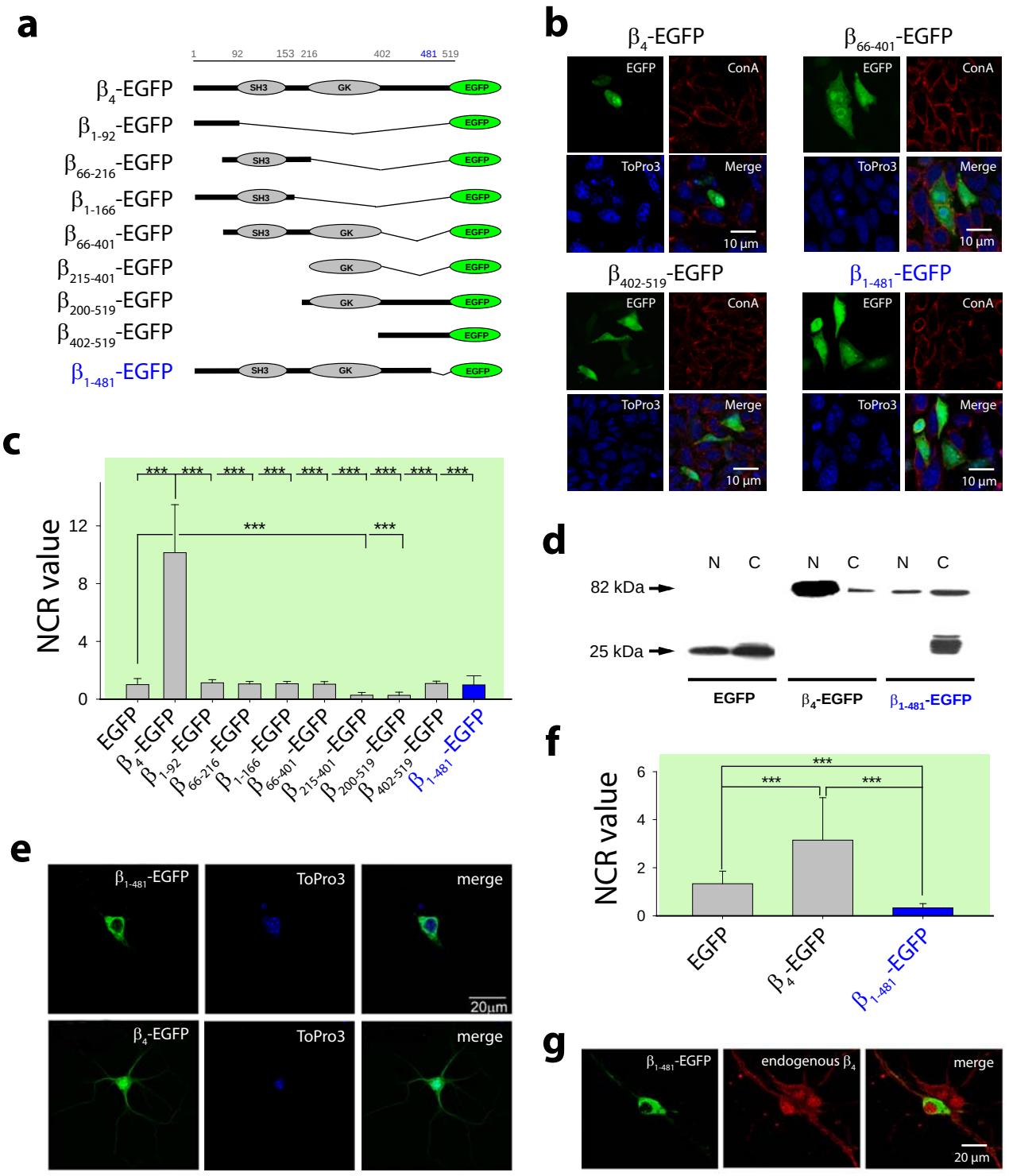

Figure 3 (De Waard)

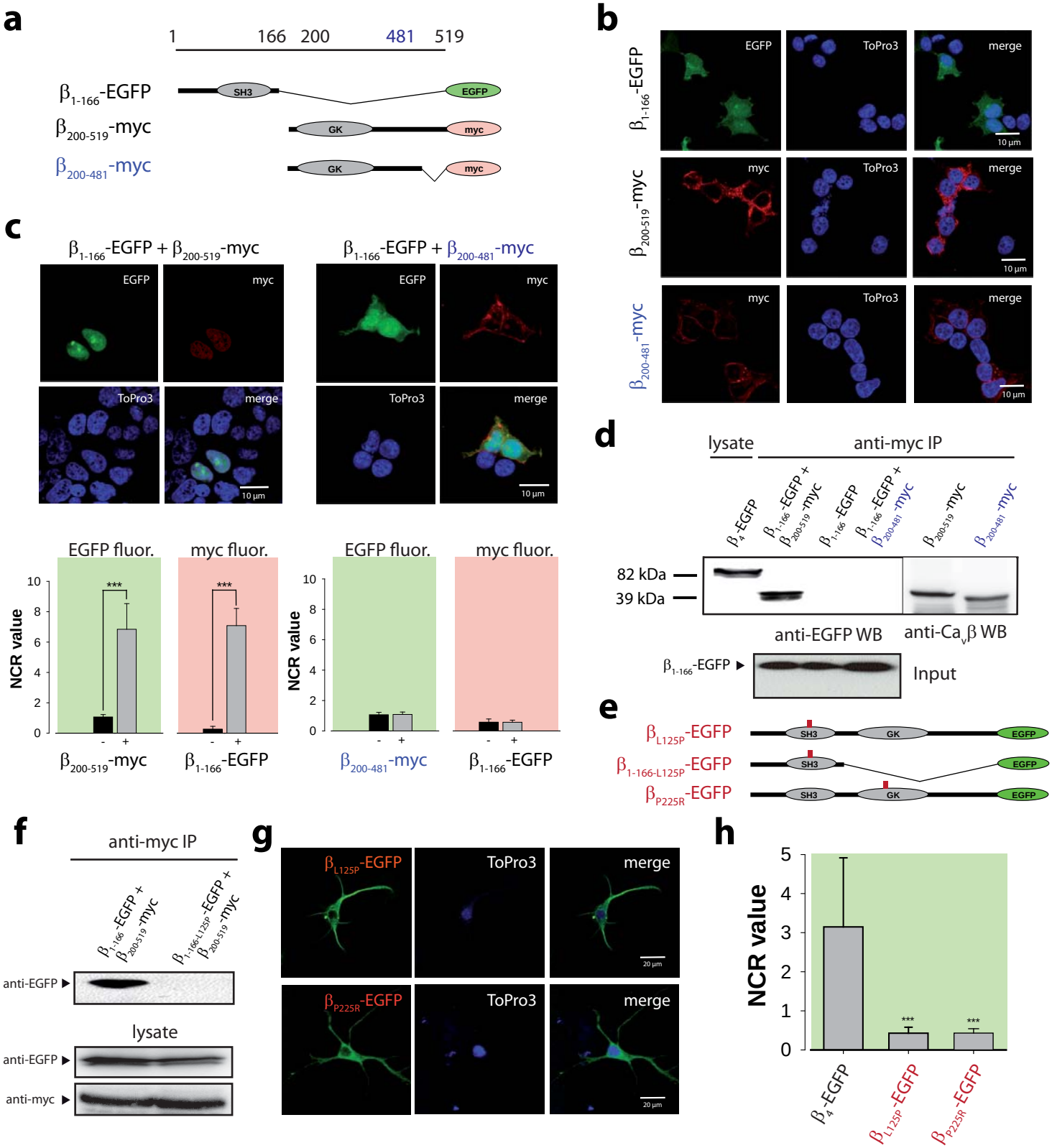

Figure 4 (De Waard)

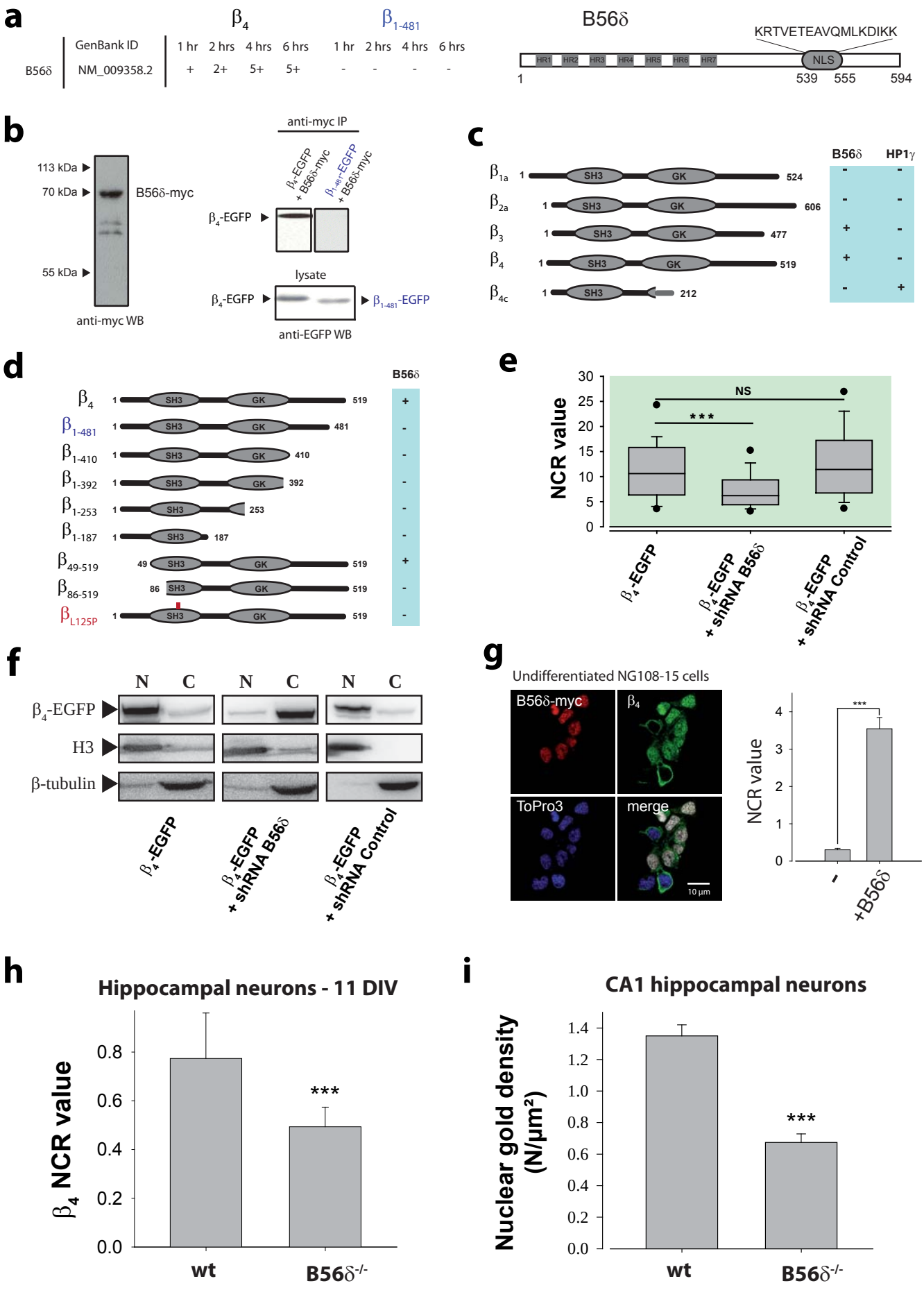

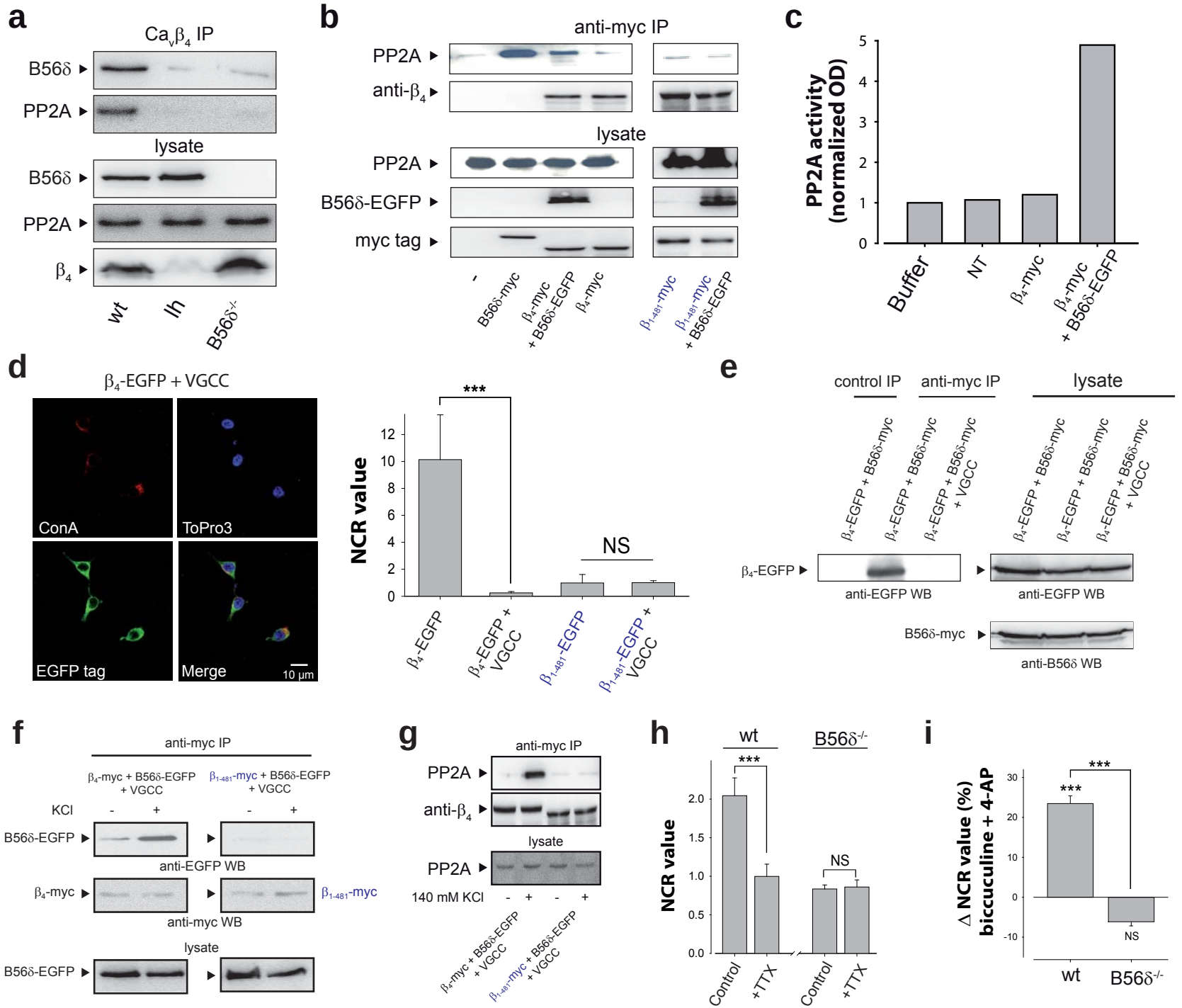
a
Ca$_v$β$_4$ IP
B56δ
PP2A
lysate
B56δ
PP2A
β$_4$
wt
Ih
B56δ$^{-/-}$
b
anti-myc IP
PP2A
anti-β$_4$
lysate
PP2A
B56δ-EGFP
myc tag
-
B56δ-myc
β$_4$-myc + B56δ-EGFP
β$_4$-myc
β$_{1-481}$-myc
β$_{1-481}$-myc + B56δ-EGFP
c
PP2A activity (normalized OD)
Buffer
NT
β$_4$-myc
β$_4$-myc + B56δ-EGFP
d
β$_4$-EGFP + VGCC
ConA
ToPro3
EGFP tag
Merge
10 µm
NCR value
***
NS
β$_4$-EGFP
β$_4$-EGFP + VGCC
β$_{1-481}$-EGFP
β$_{1-481}$-EGFP + VGCC
e
control IP
anti-myc IP
lysate
β$_4$-EGFP + B56δ-myc
β$_4$-EGFP + B56δ-myc + VGCC
β$_4$-EGFP
anti-EGFP WB
anti-EGFP WB
B56δ-myc
anti-B56δ WB
f
anti-myc IP
β$_4$-myc + B56δ-EGFP + VGCC
β$_{1-481}$-myc + B56δ-EGFP + VGCC
KCl
B56δ-EGFP
anti-EGFP WB
β$_4$-myc
β$_{1-481}$-myc
anti-myc WB
lysate
B56δ-EGFP
g
anti-myc IP
PP2A
anti-β$_4$
lysate
PP2A
140 mM KCl
β$_4$-myc + B56δ-EGFP + VGCC
β$_{1-481}$-myc + B56δ-EGFP + VGCC
h
wt
B56δ$^{-/-}$
NCR value
***
NS
Control
+TTX
Control
+TTX
i
Δ NCR value (%) biccuculine + 4-AP
***
***
NS
wt
B56δ$^{-/-}$

Figure 6 (De Waard)

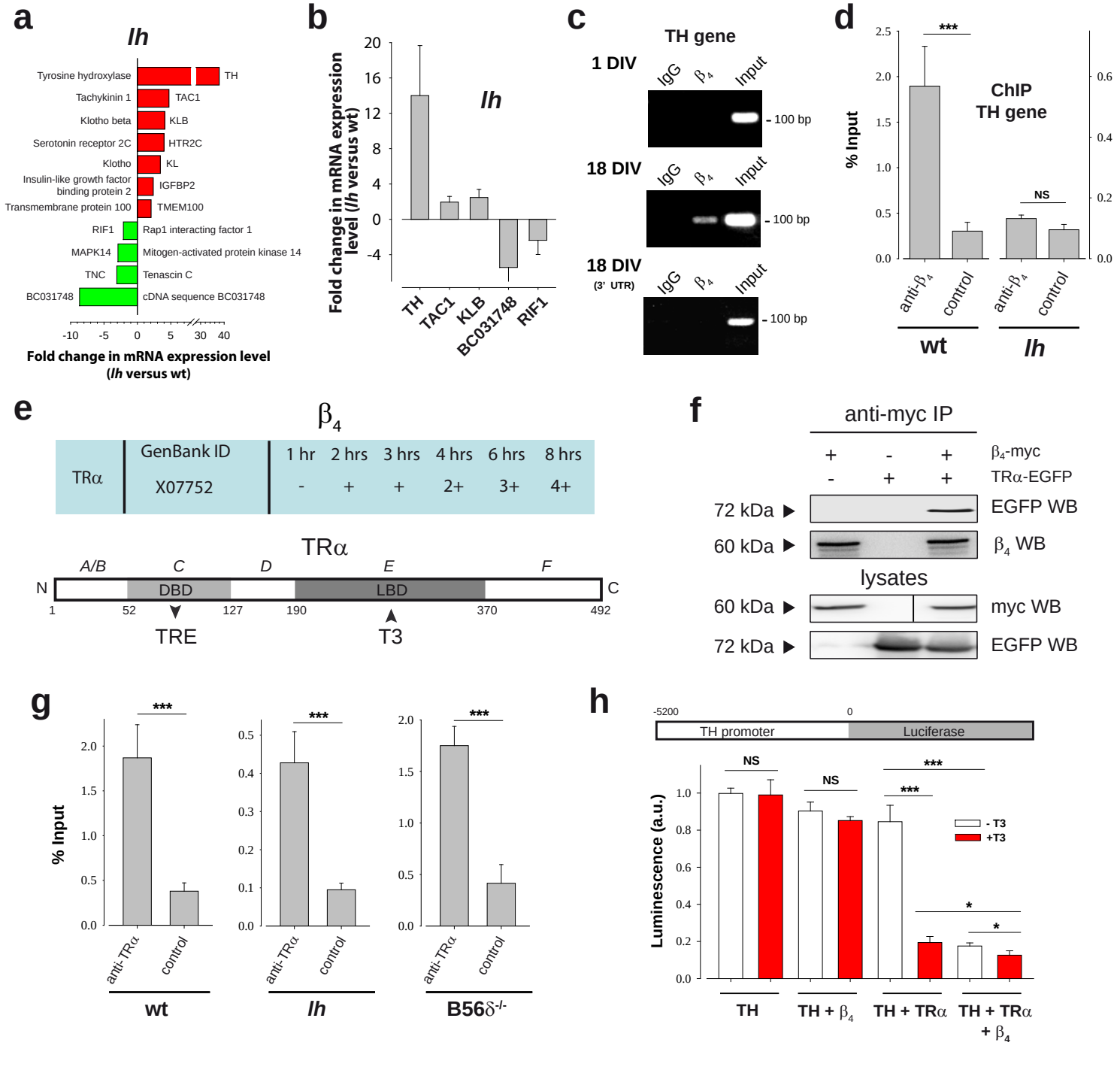

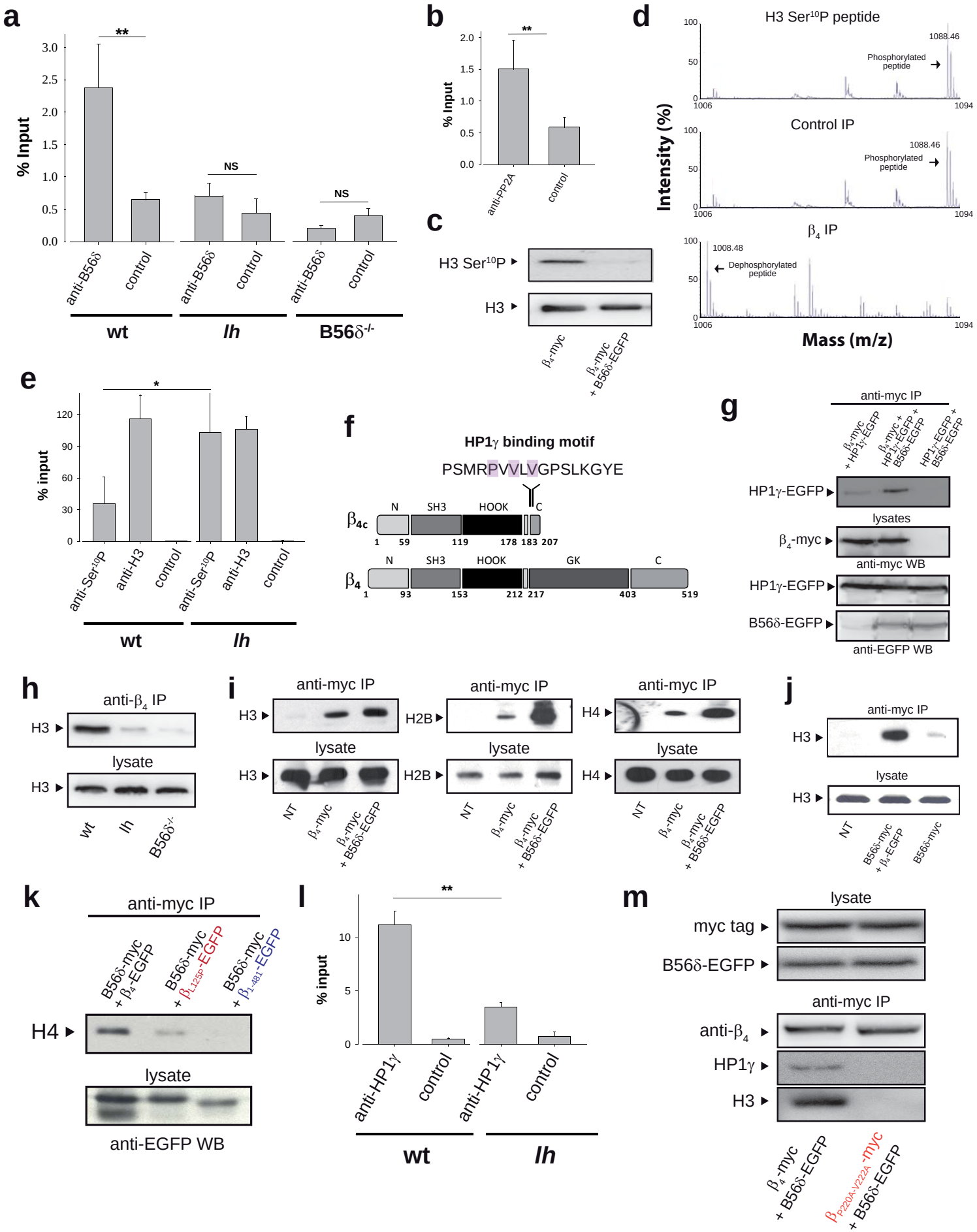
a
% Input
anti-B56δ
control
wt
lh
B56δ-/-
NS
b
% Input
anti-PP2A
control
c
H3 Ser10P
H3
β4-myc
β4-myc + B56δ-EGFP
d
H3 Ser10P peptide
1088.46
Phosphorylated peptide
Control IP
β4 IP
1008.48
Dephosphorylated peptide
Intensity (%)
Mass (m/z)
e
% input
anti-Ser10P
anti-H3
control
f
HP1γ binding motif
PSMRPVVLVGPSLKGYE
β4c
β4
N
SH3
HOOK
GK
C
g
anti-myc IP
HP1γ-EGFP
lysates
β4-myc
anti-myc WB
B56δ-EGFP
anti-EGFP WB
h
anti-β4 IP
H3
lysate
wt
lh
B56δ-/-
i
anti-myc IP
H2B
H4
NT
β4-myc
β4-myc + B56δ-EGFP
j
B56δ-myc + β4-EGFP
B56δ-myc
k
B56δ-myc + β4-EGFP
B56δ-myc + β1-123P-EGFP
B56δ-myc + β1-481-EGFP
l
anti-HP1γ
m
myc tag
B56δ-EGFP
anti-β4
HP1γ
β4-myc + B56δ-EGFP
β P220A-V222A -myc + B56δ-EGFP

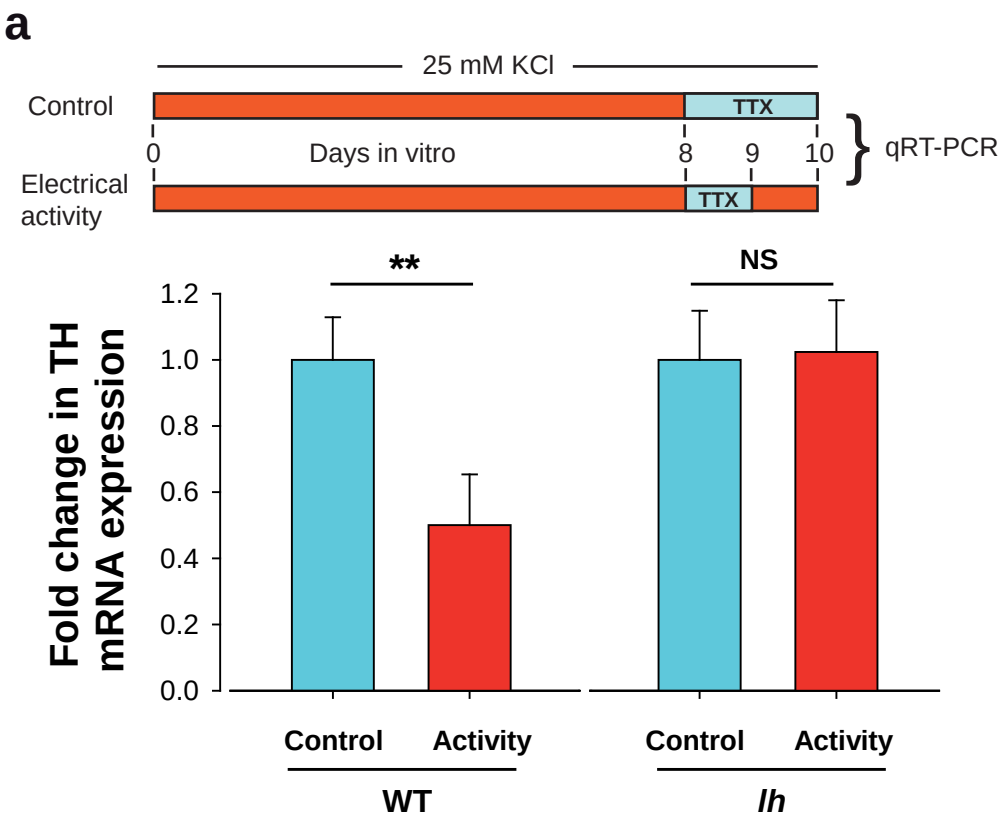
a
25 mM KCl
Control
TTX
0
Days in vitro
8
9
10
qRT-PCR
Electrical activity
TTX
**
NS
Fold change in TH mRNA expression
1.2
1.0
0.8
0.6
0.4
0.2
0.0
Control
Activity
Control
Activity
WT
lh

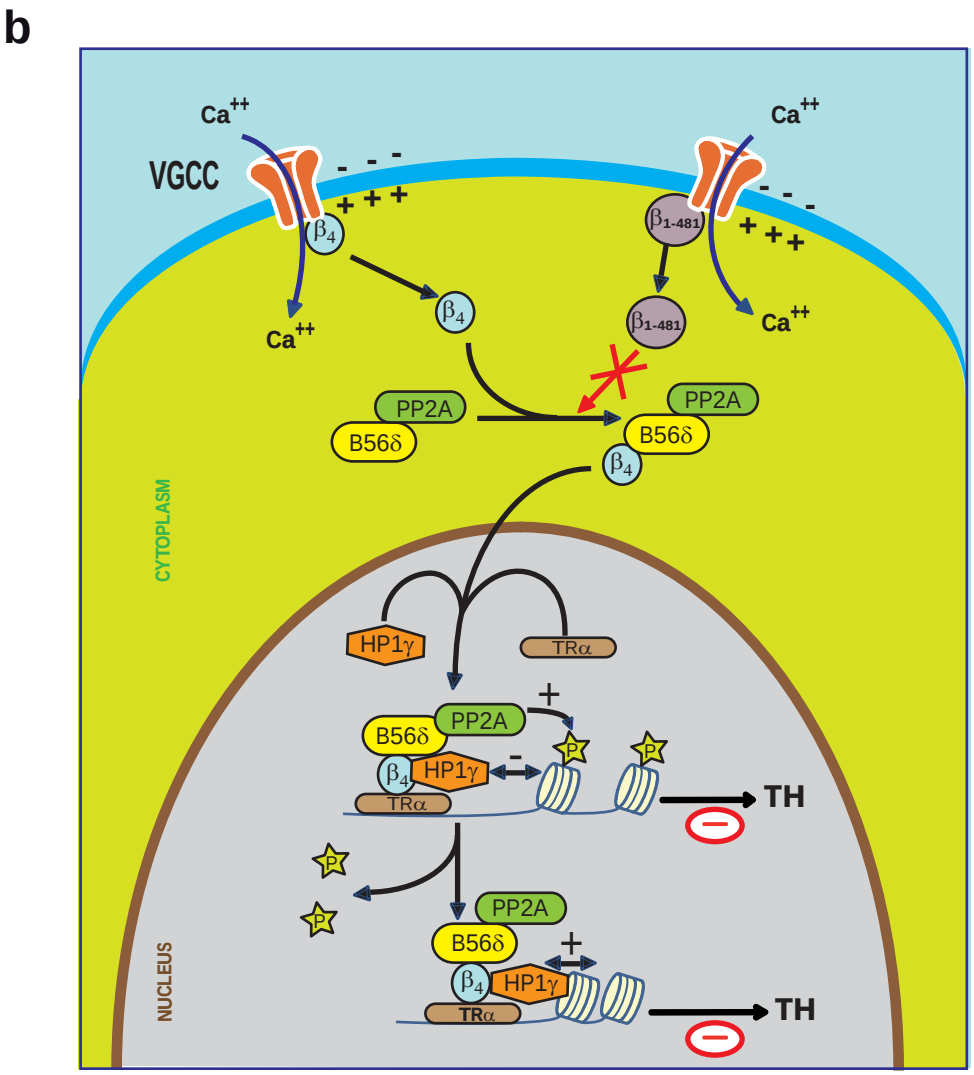
b
Ca++
VGCC
β4
Ca++
β1-481
Ca++
PP2A
B56δ
CYTOPLASM
HP1γ
TRα
TH
NUCLEUS